CPVT-associated calmodulin variants N53I and A102V dysregulate calcium signalling via different mechanisms

Ohm Prakash[1†], Marie Held[1†], Liam F. McCormick[1], Nitika Gupta[2], Lu-Yun Lian[3], Svetlana Antonyuk[4], Lee P. Haynes[2], N. Lowri Thomas[5] and Nordine Helassa[1‡]

[1]Liverpool Centre for Cardiovascular Science, Department of Cardiovascular Science and Metabolic Medicine, Institute of Life Course and Medical Sciences, Faculty of Health and Life Sciences, University of Liverpool, Liverpool L69 3BX, UK

[2]Department of Molecular Physiology and Cell signalling, Institute of Systems, Molecular & Integrative Biology, Faculty of Health and Life Sciences, University of Liverpool, Liverpool L69 3BX, UK.

[3]NMR Centre for Structural Biology, Institute of Systems, Molecular & Integrative Biology, Faculty of Health and Life Sciences, University of Liverpool, Liverpool L69 7ZB, UK

[4]Molecular Biophysics Group, Institute of Systems, Molecular & Integrative Biology, Faculty of Health and Life Sciences, University of Liverpool, Liverpool L69 7ZB, UK

[5]School of Pharmacy & Pharmaceutical Sciences, Cardiff University, Cardiff, Redwood Building, CF10 3NB, UK

[†]Authors contributed equally to the work

[‡]Corresponding author, nhelassa@liverpool.ac.uk, +44-(0)151-794-4191

Abstract

Catecholaminergic polymorphic ventricular tachycardia (CPVT) is an inherited condition that can cause fatal cardiac arrhythmia. Human mutations in the Ca^{2+} sensor calmodulin (CaM) have been associated with CPVT susceptibility, suggesting that CaM dysfunction is a key driver of the disease. However, the detailed molecular mechanism remains unclear. Focusing on the interaction with the cardiac ryanodine receptor (RyR2), we determined the effect of CPVT-associated variants N53I and A102V on the structural characteristics of CaM and on Ca^{2+} fluxes in live cells. We provide novel data showing that binding of both Ca^{2+}/CaM-N53I and Ca^{2+}/CaM-A102V to $RyR2_{3583-3603}$ is decreased. Ca^{2+}/CaM:$RyR2_{3583-3603}$ high-resolution crystal structures highlight subtle conformational changes for the N53I variant, with A102V being similar to wild-type. We show that co-expression of CaM-N53I or CaM-A102V with RyR2 in HEK293 cells significantly increased the duration of Ca^{2+} events, CaM-A102V exhibited a lower frequency of Ca^{2+} oscillations. In addition, we show that CaMKIIδ phosphorylation activity is increased for A102V, compared to CaM-WT. This paper provides novel insight into the molecular mechanisms of CPVT-associated CaM variants and will facilitate development of strategies for future therapies.

Introduction

Catecholaminergic polymorphic ventricular tachycardia (CPVT) is a genetic channelopathy which usually presents in children and young adults that can result in sudden death (Behere and Weindling, 2016). CPVT can cause syncope, severe tachyarrhythmia and cardiac arrest under the conditions of extreme physical activity or emotional stress, in structurally normal hearts (Bardai et al., 2011; Meyer et al., 2012). CPVT has an estimated incidence rate of 1:10,000 with a mortality rate of up to 13% for patients under treatment (Behere and Weindling, 2016). Mutations in the cardiac isoform of the ryanodine receptor (RyR2) are the common genetic basis for CPVT (Lanner et al., 2010; Liu et al., 2017; Priori et al., 2001; Van Petegem, 2012; Zhao et al., 2015), however recent genetic studies have identified novel calmodulin (CaM) mutations associated with the disease (Chazin and Johnson, 2020; Gomez-Hurtado et al., 2016; Jensen et al., 2018; Makita et al., 2014; Nyegaard et al., 2012; Wang et al., 2020).

In the heart, CaM is a major player in the regulation of various ion channels and pumps (Balshaw et al., 2001; Ben-Johny et al., 2015; Ben-Johny and Yue, 2014; Pitt et al., 2001; Shifman et al., 2006; Van Petegem et al., 2005; Yamaguchi et al., 2003; Zhang et al., 2012). CaM is a highly conserved calcium (Ca^{2+}) sensing protein encoded by three independent genes *CALM1*, *CALM2* and *CALM3*, and all three encode an identical 16.7 kDa, 148 amino acid long protein (Fischer et al., 1988; Toutenhoofd et al., 1998). Mutation in any of the six alleles can have critical effects on the excitation-contraction coupling process and can result in life-threatening arrhythmogenic conditions (Jensen et al., 2018; Nyegaard et al., 2012; Vassilakopoulou et al., 2015). The dumbbell-like structure of CaM comprises of four EF-hand motifs, each able to bind one Ca^{2+} ion. A flexible linker which tethers the N and C globular domains permits high conformational plasticity in binding to targets. Ca^{2+} binding at the two domains is cooperative in nature, with the N-terminal lobe showing faster Ca^{2+} binding compared to the C-terminal lobe (Zhang et al., 2012). The C-terminal lobe has 6-7 times higher Ca^{2+} binding affinity than the N-terminal lobe, thus allowing CaM to function either as a rapid or slow Ca^{2+} sensor across wide range of Ca^{2+} concentrations (Gomez-Hurtado et al., 2016; Hwang et al., 2014; Linse et al., 1991; Sondergaard et al., 2015a; Sondergaard et al., 2015b). Moreover, Ca^{2+} binding induces a large conformational transition in CaM which exposes hydrophobic patches within the helices of the EF-hands that permits the interaction with a wide range of targets.

In cardiomyocytes, during Ca^{2+}-induced Ca^{2+} release (CICR), membrane depolarisation activates voltage-gated Ca^{2+} channels ($Ca_v1.2$) which causes extracellular Ca^{2+} to enter the cell. Increase in local Ca^{2+} concentrations triggers the release of Ca^{2+} from the sarcoplasmic reticulum (SR) through RyR2 (Dewenter et al., 2017; Endo, 1977). Diffusion of this cytoplasmic Ca^{2+} into the myofibrils promotes the interaction between actin and myosin that results in heart muscle contraction. Tightly controlled cycling of intracellular Ca^{2+} concentration is the basis of normal heart rhythm (Bootman et al., 2002; Landstrom et al., 2017; Luo and Anderson, 2013). The open probability of RyR2 in response to variations in cytoplasmic Ca^{2+} concentration is regulated by both Ca^{2+} free (apo-) and Ca^{2+}/CaM (Balshaw et al., 2001; Balshaw et al., 2002; Brohus et al., 2019; Sigalas et al., 2009; Walweel et al., 2017; Xu and Meissner, 2004; Yamaguchi et al., 2007; Yamaguchi et al., 2003; Yang et al., 2014), however the effect of CPVT-associated CaM mutations on CaM:RyR2 function remains unclear. In order to determine the molecular mechanism leading to CPVT, a detailed functional, biophysical and structural characterisation of the interaction between CaM and RyR2 is required.

Here we report the results from a comprehensive analysis of the interaction between CaM CPVT-associated variants – CaM-N53I and CaM-A102V – and the RyR2 CaM binding domain (CaMBD). CaM N53I variant was discovered in a large Swedish family with a severe dominantly inherited form of CPVT-like arrhythmias. Using a genome-wide linkage analysis, they demonstrated that the heterozygous missense mutation in the gene encoding calmodulin (*CALM1*) segregated with the disease and showed compromised calcium binding (Nyegaard et al., 2012). CaM A102V variant was identified in *CALM3* in a female who experienced episodes of exertion-induced syncope since age 10, had normal QT interval, and displayed ventricular ectopy during stress testing consistent with CPVT. CaM-A103V was shown to lower CaM Ca^{2+}-binding affinity and promoted spontaneous Ca^{2+} wave and spark activity in permeabilised cardiomyocytes (Gomez-Hurtado et al., 2016).
In this paper, we provide high-resolution 3D structures of CaM variants in complex with $RyR2_{3583-3603}$ and novel data on the binding mechanism of CaM to RyR2. We show for the first time that arrhythmogenic variants N53I and A102V alter intracellular Ca^{2+} oscillations kinetics and can significantly increase CaMKIIδ phosphorylation activity. Collectively, these data provide novel insight into the molecular aetiology of CPVT with abnormal Ca^{2+} release from SR via distinct molecular mechanisms for N53I and A102V.

Results

CPVT-associated CaM variants have reduced affinity for RyR2 CaMBD in the presence of Ca^{2+}.
Both apo- and Ca^{2+}/CaM are known to directly bind the RyR2-CaMBD (3583-3603) to regulate the gating activity of the channel. To analyse the effect of CPVT-associated mutations on CaM:$RyR2_{3583-3603}$ interaction, we carried out isothermal titration calorimetry (ITC) experiments in the absence (5 mM EGTA) and presence of activating Ca^{2+} concentration (5 mM $CaCl_2$). ITC provides value for the dissociation constant (K_d), stoichiometry of binding (N), and can reveal the nature of the forces that drive the binding reaction (enthalpy change, ΔH and the entropic term, ΔS).
CaM binding to $RyR2_{3583-3603}$ has a stoichiometry of 1:1 in both apo and Ca^{2+} conditions (Fig. 1A,B). In the absence of Ca^{2+}, K_d of CaM-WT for $RyR2_{3583-3603}$ is 15 ± 3 μM. CPVT-associated variants (N53I and A102V) did not significantly alter the affinity with K_d of 10 ± 1 μM and 15 ± 2 μM, respectively (Fig. 1C). However, in the presence of Ca^{2+}, the affinity for $RyR2_{3583-3603}$ was significantly reduced by up to 7-fold when compared to CaM-WT from 51 ± 9 nM (CaM-WT) to 146 ± 40 nM (CaM-N53I) and 349 ± 72 nM (CaM-A102V) (Fig. 1D).
The Gibbs free energy change (ΔG) for CaM:$RyR2_{3583-3603}$ interaction in both apo and Ca^{2+} conditions is negative which is characteristic of a spontaneous, favourable reaction for all CaM variants (Fig. 1C,D). For apo-CaM:$RyR2_{3583-3603}$, the interaction is endothermic and entropy driven (Fig. 1A,C), suggesting an important contribution of hydrophobic interactions. In contrast, the Ca^{2+}/CaM:$RyR2_{3583-3603}$ interaction is exothermic and enthalpy driven (Fig. 1B,D). Interestingly, while Ca^{2+}/CaM-WT:$RyR2_{3583-3603}$ binding shows favourable entropy, the CPVT variants show unfavourable entropy, indicating a different binding mechanism.

Secondary structure of CaM is not affected for the CPVT-associated variants.
We employed circular dichroism (CD) spectroscopy in order to determine whether CPVT-associated CaM variants induced differences in secondary structure distributions (Fig. 2A,B). In Ca^{2+}-free conditions, the α-helical content of CaM-WT was predicted to be 43 ± 1% α-helices and 11 ± 2% β-sheets. Upon binding to Ca^{2+}, the CaM proteins underwent

conformational changes with a significant increase in α-helix content (51-54%) measured in all CaM proteins. The CPVT-associated variants did not show significantly altered secondary structure content of CaM in apo- or Ca^{2+}-saturating conditions when compared to the wild-type protein.

N53I and A102V CaM variants showed altered protein stability.

To determine whether activating levels of Ca^{2+} and/or RyR2 binding induced significant conformal changes that would affect susceptibility to proteases, we employed a biochemical assay using the endoproteinase AspN (Fig. S1A,B). In apo conditions, we observed that over 97% of CaM proteins were degraded when incubated with 0.6 $\mu g.mL^{-1}$ AspN (Fig. S1A). Complex formation between apo-CaM and $RyR2_{3583-3603}$ induced a significant resistance to protease cleavage, with 5.0 $\mu g.mL^{-1}$ required to degrade over 90% of wild-type and A102V CaM proteins. The apo-CaM-N53I:$RyR2_{3583-3603}$ variant exhibited a substantial increase in stability, requiring 10.0 $\mu g.mL^{-1}$ of AspN to achieve similar levels of degradation as the apo-CaM-WT:$RyR2_{3583-3603}$ and apo-CaM-A102V:$RyR2_{3583-3603}$ complexes.

Ca^{2+}/CaM proteins showed a significant reduction in susceptibility to AspN cleavage with 500 times more AspN protease (300 $\mu g.mL^{-1}$) required to achieve full degradation, when compared to apo-CaM. Ca^{2+}/CaM-N53I showed an increased susceptibility to AspN degradation when compared to the A102V and wild-type forms (Fig. S1B). Complex formation of Ca^{2+}/CaM with $RyR2_{3583-3603}$ again increased the stability of CaM with only 19 ± 2 % of the wild-type degraded at high AspN concentrations (300 $\mu g.mL^{-1}$) and the CPVT-associated variants did not induce any significant differences.

Interestingly, despite the susceptibility to protease degradation not being different for the apo-CaM species, we observed that the CPVT-associated variants have significantly reduced temperature stability. The melting temperature (T_m) assessed by circular dichroism decreased from 41.6 ± 0.3 °C to 37.0 ± 0.7 °C (N53I) and 39.3 ± 0.4 °C (A102V) (Fig. S1C).

CPVT-associated mutations N53I and A102V induce subtle local structure perturbations.

Two-dimensional ^{1}H-^{15}N HSQC NMR was used to investigate the effect of the mutations on the 3D structure of Ca^{2+}/CaM. We were able to unambiguously assign 144 of 148 (minus two proline residues, Asn42 and Met76) backbone resonances for Ca^{2+}/CaM-WT. Over 92% of wild-type resonance assignments were transferred to both CaM-N53I and CaM-A102V HSQC spectra.

Comparison of chemical shifts between CaM-WT and CaM-N53I spectra revealed, as expected, significant perturbations of chemical shifts around the site of amino acid substitution with the largest shift difference occurring at Val55 (0.146 ppm) (Fig. 2C). The residues Thr26-Gly33 and Val55-Ala57 showed noticeable chemical shifts with additional shift changes detected for more distal residues Met71 and Ser101.

On the other hand, the shift differences of CaM-A102V revealed a more localised effect when the shift perturbations (A102V vs WT) were mapped onto the protein structure (Fig. 2D). The residues with large chemical shifts were confined to the C-terminal region: Lys94, Arg106, Thr110, Glu114, Leu116, Ile130, and Asn137. Most differences were observed around the site of mutation located at the third EF-hand motif (largest shift changes in Thr110, 0.135 ppm), with fewer residues substantially perturbed at the neighbouring Ca^{2+} binding motif. Despite variations in the chemical shift perturbations in the two variants, larger chemical shift changes appeared to localise within the respective lobe at which they occurred. This indicates that the CPVT-associated mutations do not globally remodel protein structure but induce localised changes to protein architecture, particularly at the sites responsible for Ca^{2+} co-ordination.

The C-lobe of Ca^{2+}/CaM forms the initial site of interaction with RyR2.
Using two-dimensional ^{1}H-^{15}N HSQC NMR and stepwise titration of the $RyR2_{3583-3603}$ peptide to Ca^{2+}/CaM, we were able track the changes in chemical shifts and deduce structural information about how the complexes between CaM and RyR2 are formed.

At one molar equivalent peptide, 46 % of the backbone resonances were assigned; the same percentage of residues were also assignable for the CaM-N53I and CaM-A102V variants.
Upon the addition of one equivalent $RyR2_{3583-3603}$ peptide to CaM-WT, residues from the C-lobe were twice as likely to be affected by the presence of the peptide than the N-lobe residues (Table S1). Only 29% of the resonances from the C-lobe compared with 57% from the N-lobe, were not affected by the presence of the peptide. Interestingly, when the $RyR2_{3583-3603}$ peptide is added to two molar equivalents, we observed the opposite effect: 58% and 92% of the resonances in the N and C lobes respectively, were not significantly perturbed. Therefore, the C-lobe residues appear to be more affected at lower concentrations of the peptide, whereas those the N-lobe respond when the peptide is at a higher concentration. The same chemical shift perturbation phenomenon is also observed for CaM-N53I and CaM-A102V. These data suggests that in all three Ca^{2+}/CaM forms, the C-lobe form the initial site of interaction.
From the titration experiments, CaM-N53I and CaM-A102V do not result in altered complex formation with the $RyR2_{3583-3603}$ peptide. Binding of the peptide occurs via the C-lobe initially followed by N-lobe conformational changes as evidenced by the chemical shifts analysis.

Crystal structure of Ca^{2+}/CaM-N53I:$RyR2_{3583-3603}$ shows subtle conformational changes when compared to wild-type.
We co-crystallised Ca^{2+}/CaM variants, with the $RyR2_{3583-3603}$ peptide to gain an atomistic understanding of the interaction. Ca^{2+}/CaM-WT:$RyR2_{3583-3603}$ (PDB 6XXF), Ca^{2+}/CaM-N53I:$RyR2_{3583-3603}$ (PDB 6XY3) and Ca^{2+}/CaM-A102V:$RyR2_{3583-3603}$ (PDB 6XXX) crystal structures were solved to a high resolution of 1.70 Å, 2.00 Å and 1.25 Å respectively (Fig. 3A-C). Crystallographic data and refinement statistics are given in Table S2. All the complexes gave clear electron density for four Ca^{2+} ions at the N- and C-terminal Ca^{2+} binding grooves. To determine the effect of CPVT-associated mutations on the structure of Ca^{2+}/CaM-$RyR2_{3583-3603}$ complexes, we compared Ca^{2+}/CaM-WT:$RyR2_{3583-3603}$ with Ca^{2+}/CaM-N53I:$RyR2_{3583-3603}$ and Ca^{2+}/CaM-A102V:$RyR2_{3583-3603}$ peptide complex crystal structures obtained in this study (Fig. 3D-E). The interactions between CaM residues and Ca^{2+} ions were conserved and identical in all the structures. In addition to the overall structural superimposition, we superimposed individual regions of the Ca^{2+}/CaM:$RyR2_{3583-3603}$ peptide complex to specific domains in order to identify the region with considerable structural root mean square deviation (RMSD) (Fig. S2A-B, Table S3). The overall structure of all the compared complexes showed similar conformation to the Ca^{2+}/CaM-WT:$RyR2_{3583-3603}$ peptide complex. Based on the RMSD values, the flexible helix region seems to contribute the most towards the observed small structural discrepancy.

CPVT mutations induce subtle changes in hydrophobic, hydrogen and salt bridge interactions in Ca^{2+}/CaM:RyR structures.
The Ca^{2+}/CaM-WT:$RyR2_{3583-3603}$ and Ca^{2+}/CaM-N53I:$RyR2_{3583-3603}$ peptide complex structure show subtle differences at mutation region (Fig. 4A,B). However, these differences do not result in major structural differences in $RyR2_{3583-3603}$ peptide binding (Table S3, RMSD 1.31 Å), with the prominent difference is the side chain orientation of amino acid Glu54 and the disruption of the hydrogen bonding network near Ile53 (Fig. 4A,B). In the

Ca^{2+}/CaM-WT:$RyR2_{3583-3603}$ structure, atoms $N^{\delta 2}$ Asn53 and N Asn53 form a direct hydrogen bond with O of another CaM residue, Gln49. $O^{\delta 1}$ Asn53 also forms hydrogen bond with $O^{\delta 2}$ Asp56 through a water molecule W1. Asp56 in turn is involved in Ca^{2+} binding in the EF-hand (Fig. 4A). In Ca^{2+}/CaM-N53I:$RyR2_{3583-3603}$, the main chain atoms N Ile53 and O Gln49 interactions are retained. However, since isoleucine (Ile/I) is a hydrophobic amino acid in contrast to asparagine (Asn/N) which is polar hydrophilic, the water molecule W1, which forms part of the hydrogen bond network is lost in the N53I mutant CaM. Interestingly, O Ile53 then forms a direct hydrogen bond with N Asp56 (Fig. 4B). We observed that the Ca^{2+}/CaM-A102V:$RyR2_{3583-3603}$ complex is structurally very similar to Ca^{2+}/CaM-WT:$RyR2_{3583-3603}$ (Fig. 3E, Fig. S2B, Table S3, RMSD 0.63 Å). Even though no major structural difference could be discerned at the vicinity of the mutation, the A102V substitution increases interaction surface hydrophobicity when compared with Ca^{2+}/CaM-WT:$RyR2_{3583-3603}$ structure (Fig. 4C-D).

The H-bond and salt bridge interactions between the Ca^{2+}/CaM and the corresponding peptides were predicted by the PDBePISA server (Krissinel and Henrick, 2007). Although most of the interactions are conserved in all the complexes, subtle differences in the side chain orientations changes the individual atoms involved in interactions (Table S4). Residues from Ca^{2+}/CaM and corresponding peptides involved in H-bonds and salt bridges unique to each are represented in Figure S3.

CPVT-associated CaM variants N53I and A102V differentially modulate Ca^{2+}/CaM kinase II (CaMKIIδ) phosphorylation activity.

Using radiolabelled ATP and mice heart lysate as a source of CaMKIIδ, phosphorylation levels of syntide-2 (CaMKIIδ substrate) were measured using wild-type and CPVT-associated CaM variants (SignaTECT, Promega). We showed that, when using CaM-N53I as CaMKIIδ activator, phosphorylation of syntide-2 remained unaffected while CaM-A102V significantly increased phosphorylation levels by 57 ± 17%, when compared to CaM-WT (Fig. 5A).

Using commercial human CaMKIIδ recombinant protein (Abcam, ab84552), the rate of Thr^{287} autophosphorylation for Ca^{2+}/CaM.CaMKIIδ was estimated by western blot and densitometry analysis (Fig. 5B). We did not observe significant difference between CaM-WT and disease-associated mutants, demonstrating that the increase in phosphorylation activity observed for CaM-A102V cannot be attributed to enhanced autophosphorylation.

CaM-N53I and A102V alter spontaneous Ca^{2+} signalling events in cells.

To assess the effect of CPVT-associated CaM mutations on Ca^{2+} release from the endoplasmic reticulum (ER), we transiently over-expressed human RyR2 and CaM variants in HEK293T cells. Using Calbryte 520 as a Ca^{2+} indicator, we measured spontaneous Ca^{2+} oscillations using single-cell fluorescence confocal microscopy. Cells which exhibited regular spontaneous Ca^{2+} release events, indicative of functional RyR2 expression (Jiang et al., 2004) were included in the analysis of kinetic parameters (Fig. 6). Co-expression of CaM-WT with RyR2 decreased the amplitude of Ca^{2+} transients and affected their duration, making them significantly shorter, to the extent that the frequency of events was increased, with the interval between release events (inter-transient interval) shorter to that in cells expressing RyR2 alone.

CPVT-associated CaM mutations did not affect amplitude, inter-transient interval, ER load, rise and fall rate of RyR2-mediated Ca^{2+} release events compared to CaM-WT. However, CaM-N53I and A102V resulted in a significant increase in duration of the events, which significantly reduced the frequency for CaM-A102V (Fig. 6 and Fig. S4A).

We did not observe any significant effect of the CaM mutations on intra-cellular Ca^{2+} concentrations and non-RyR associated Ca^{2+} responses when stimulated with the muscarinic receptor agonist, carbachol or the SERCA inhibitor, thapsigargin (Fig. S4B-D).

Discussion

CaM is an ubiquitously expressed Ca^{2+} sensor that regulates several target proteins involved in excitation-contraction coupling in the heart including RyR2 and $Ca_v1.2$ (Balshaw et al., 2001; Hoeflich and Ikura, 2002; Kim et al., 2004; Lanner et al., 2010; Pitt et al., 2001; Yamaguchi et al., 2003; Yang et al., 2003). CaM modulates RyR2-mediated Ca^{2+} release from the SR either via direct inhibition of RyR2 or indirectly via phosphorylation of RyR2 by Ca^{2+}/CaM kinase II (CaMKIIδ) (Ai et al., 2005; Walweel et al., 2019; Walweel et al., 2017). Finely tuned CaM-RyR2 interaction is essential for normal SR Ca^{2+} release and heart function. Abnormal interaction between CaM and RyR2 due to mutations in the CaMBD of RyR2 or in CaM itself can cause severe cardiac complications including cardiac hypertrophy, heart failure and arrhythmias such as CPVT (Balshaw et al., 2001; Yamaguchi et al., 2013; Yamaguchi et al., 2007). In this paper, we used a multidisciplinary approach combining protein biophysics, structural biology and Ca^{2+} imaging to determine the effect of the CPVT-associated CaM variants N53I and A102V on CaM:RyR2 structure-function relationship. The major biophysical properties from this work of CPVT-associated CaM variants in comparison to CaM-WT are summarized in Table 1.

Disease-associated mutations can affect protein folding and/or reduce protein stability leading to protein dysfunction. In accordance with previous studies investigating CaM-N53I, we showed that the secondary structure of the CaM-N53I variant was unchanged (Sondergaard et al., 2015a; Vassilakopoulou et al., 2015) and observed a reduced thermal stability (Sondergaard et al., 2015a), when compared to CaM-WT. We demonstrated that conformational change adopted by CaM in the presence of Ca^{2+} and/or RyR2 protected the protein against protease degradation (AspN), suggesting a significant change in local intramolecular dynamics of the protein. In all conditions tested, A102V susceptibility to proteases was similar to CaM-WT, indicating that only the N53I variant induced subtle but notable structural changes.

Using ITC, we determined for the first time the binding and thermodynamic properties of CaM A102V:$RyR2_{3583-3603}$. We showed that the interaction of apo-CaM-WT with $RyR2_{3583-3603}$ is entropy driven (hydrophobic interaction) with a K_d of 15 ± 3 μM. In the absence of Ca^{2+}, the CPVT-associated variants N53I (Holt et al., 2020) and A102V did not significantly affect the affinity. For Ca^{2+}/CaM, interaction with $RyR2_{3583-3603}$ is enthalpy driven and K_d is significantly decreased from 15 ± 3 μM to 52 ± 4 nM, as previously shown (Holt et al., 2020; Lau et al., 2014). In contrast to other studies which did not show any difference in binding affinity of Ca^{2+}/CaM-N53I and Ca^{2+}/CaM-A102V for RyR2 (Gomez-Hurtado et al., 2016; Holt et al., 2020), we observed a significant 3- and 7-fold decrease in affinity for N53I and A102V, respectively. Using similar experimental conditions to Holt and coworkers (longer RyR2 peptide $RyR2_{3581-3608}$ and absence of magnesium), we still observed significant reduced affinities for the disease-associated CaM mutants (Fig. S5).
Ca^{2+}/CaM-WT:$RyR2_{3583-3603}$ binding showed favorable entropy suggesting an important contribution of hydrophobic interactions, whereas the CPVT variants have unfavorable entropy indicating a different binding mechanism comprising of hydrogen and Van der Waals bonds which can account for the measured reduction in affinity. Upon Ca^{2+} binding, CaM

undergoes a conformational switching which drives target binding. Interestingly, it has been shown that the N53I mutation did not significantly alter Ca^{2+} affinity (Hwang et al., 2014; Vassilakopoulou et al., 2015) whereas CaM-A102V has a 3-fold larger K_d for Ca^{2+} (Gomez-Hurtado et al., 2016). The impaired Ca^{2+} binding can affect CaM structural transitions and thus subsequent interactions with its target RyR2. Altogether, our data indicate that in regard to the physiology of CPVT, pre-association of CaM to RyR2 is not altered; however, when intracellular Ca^{2+} increase during CICR, the decreased affinity for RyR2 reduces the inhibition of the channel and can promote Ca^{2+} release from the SR.
In CaM-associated CPVT syndromes, only one out of six CaM alleles are mutated. However it has been shown that in the presence of 3-fold excess of CaM-WT, the variants CaM N53I and CaM-A102V can promote significantly higher Ca^{2+} wave frequencies in permeabilized cardiomyocytes, when compared to CaM-WT (Gomez-Hurtado et al., 2016; Hwang et al., 2014). These data demonstrate that CPVT-associated CaM mutations can lead to a dominant pathogenic effect, which is consistent with an autosomal dominant inheritance pattern in humans. The functional dominance can be explained by the fact that the tetrameric RyR2 Ca^{2+} channel has four CaM binding sites and binding of only one single mutant CaM may be sufficient to disrupt the CaM-dependent regulation of Ca^{2+} release from the SR.

We investigated the dynamics and atomistic details of Ca^{2+}/CaM:$RyR2_{3583-3603}$ interaction by NMR spectroscopy and X-ray crystallography. This revealed for the first time the stages of Ca^{2+}/CaM:$RyR2_{3583-3603}$ complex formation through two-dimensional ^{1}H-^{15}N HSQC NMR. The binding event is initiated by the C-terminal region of CaM and further completed by the N-terminal region. This dynamic characteristic of Ca^{2+}/CaM:$RyR2_{3583-3603}$ peptide complex formation is conserved across all the CaM variants (WT, N53I and A102V).
The NMR chemical shift perturbations of the variants show that in addition to the residues which are sequentially and spatially close the mutated residues being affected, more spatially distant residues also undergo shift perturbations. This indicates some intramolecular structural rearrangements of the tertiary structures in the variants.

We deposited high-resolution structures for Ca^{2+}/CaM-WT bound to $RyR2_{3583-3603}$ (PDB 6XXF), Ca^{2+}/CaM-N53I:$RyR2_{3583-3603}$ (PDB 6XY3) and Ca^{2+}/CaM-A102V:$RyR2_{3583-3603}$ (PDB 6XXX). Superimposition of Ca^{2+}/CaM-WT:$RyR2_{3583-3603}$ and Ca^{2+}/CaM-N53I:$RyR2_{3583-3603}$ showed subtle structural variations whereas Ca^{2+}/CaM-A102V:$RyR2_{3583-360}$ is more similar to the wild-type structure (lower structural RMSD between individual domains). The largest structural RMSD was observed at the linker helix domain of CaM, with some of the residue side chains not fully resolved in the X-ray structures due to their enhanced flexibility. This region is known to be highly flexible and plays a role in the structural transition of CaM upon Ca^{2+} and target binding. The hydrophobic nature of the mutant residues causes changes with respect to hydrogen bond network and side-chain orientations at the site of mutation. Since Ile has a larger hydrophobicity index value than Val residue (1.38 > 1.08) (Eisenberg, 1984), these differences are more prominent in CaM-N53I than in CaM-A102V. These localized changes did not affect the peptide binding nor the overall architecture of the Ca^{2+}/CaM:$RyR2_{3583-3603}$ complex, which agrees with the recent structures deposited by Holt and coworkers (Holt et al., 2020). However, intramolecular dynamic changes within the local environment at the site of mutation could affect the functional outcome of the interaction. The H-bond and salt bridge interactions between the CaM variants and $RyR2_{3583-3603}$ peptide showed subtle differences. We observed unique H-bond interactions in Ca^{2+}/CaM-N53I:$RyR2_{3583-3603}$ complex involving residues Glu84, Leu39 from CaM with Arg3597, Arg3595 from RyR2. Since electron density for side chain of Glu123 and Lys75 was not present in the X-ray structure of Ca^{2+}/CaM-N53I:$RyR2_{3583-3603}$,

the interaction of these residues could not be deciphered. The salt bridge interactions in Ca^{2+}/CaM-N53I:$RyR2_{3583-3603}$ showed no differences compared to Ca^{2+}/CaM-WT:$RyR2_{3583-3603}$ complex. For the Ca^{2+}/CaM-A102V:$RyR2_{3583-3603}$ complex, the H-bond network is more similar to Ca^{2+}/CaM-WT:$RyR2_{3583-3603}$ with just a single extra interaction (Met144-His3588) and a single lost interaction (Asn111-Arg3597). In the Ca^{2+}/CaM-A102V:$RyR2_{3583-3603}$ complex, Lys148 forms an extra salt-bridge interaction with His3588 in RyR2, and the interaction of residue Glu11 with Arg3595 in RyR2 is absent.

Phosphorylation of the RyR2 channel is an important prerequisite for the inhibitory CaM regulation in healthy human hearts (Walweel et al., 2019). One of the major kinases involved in RyR2 channel phosphorylation is CaMKIIδ (Edman and Schulman, 1994; Hoch et al., 1999; Hund and Mohler, 2015). Phosphorylation of RyR2 channel by CaMKIIδ subsequently escalates the RyR2-mediated SR Ca^{2+} leak and delayed afterdepolarizations (Liu et al., 2011; Wehrens et al., 2004). CaMKIIδ is a multifunctional Ser/Thr protein kinase that modulates RyR2 and $Ca_v1.2$ activity. Upon Ca^{2+}-CaM activation, this multimeric holoenzyme can first autophosphorylate and then phosphorylate target channels to regulate their function (Hudmon et al., 2005; Lanner et al., 2010; Lucic et al., 2008; Rodriguez et al., 2003; Wehrens et al., 2005; Wehrens et al., 2004; Witcher et al., 1991; Witcher et al., 1992). It has been shown using the genetically encoded sensor "Camui" that CaMKII activity was decreased in IVF and LQTS (Berchtold et al., 2016; Hwang et al., 2014). However, very limited information exists on the effect of CaM mutations on CaMKIIδ activity in CPVT. Using radiolabelled [γ^{32}P] ATP and syntide-2 as a model CaMKIIδ substrate, we showed that Ca^{2+}/CaM-N53I did not affect the kinase action of CaMKIIδ, as previously shown (Berchtold et al., 2016). However, we showed for the first time that Ca^{2+}/CaM-A102V significantly increased the substrate phosphorylation levels by ~60%. These novel data suggest a distinct mechanism of RyR2 channel inhibitory action by CaM-N53I and CaM-A102V in CPVT potentially via differential CaMKIIδ activation.

CPVT-associated CaM mutations have been shown to evoke arrhythmogenic Ca^{2+} waves in cardiomyocytes (Gomez-Hurtado et al., 2016; Hwang et al., 2014). In HEK293 cells expressing murine RyR2, Sondergaard and coworkers measured the effect of various arrhythmogenic CaM variants on ER Ca^{2+} concentration using the FRET probe D1ER. They showed that CaM variants such as A102V can decrease RyR2 activation/termination thresholds during store-overload-induced Ca^{2+} release (SOICR) (Sondergaard et al., 2019). In addition, it has been shown that N53I and A102V variants increased RyR2 open probability (*Po*) (Sondergaard et al., 2019; Sondergaard et al., 2016). However, the effect of the CaM variants on the Ca^{2+} oscillation kinetic parameters, as we demonstrate in this study, was not investigated. To determine the effect of the N53I and A102V CaM mutations on RyR2 function and Ca^{2+} fluxes, we performed a detailed analysis of spontaneous Ca^{2+} release events in HEK293T cells co-expressing human RyR2 and the CaM variants. Co-expression of CaM-WT with RyR2 decreased the amplitude of spontaneous Ca^{2+} signaling events, reduced their duration and the inter-transient interval compared to cells expressing RyR2 alone. This is consistent with an inhibitory effect of CaM on the channel, decreasing the channel open time (Xu and Meissner, 2004). As this represents a partial reversion of the Ca^{2+} release phenotype to that in the absence of CaM co-expression (i.e. RyR2 alone), this suggests that CPVT-associated mutations induce a loss of inhibitory action of the channel. In this study, we provided novel data showing a significant increase in duration of the Ca^{2+} events for both CaM-N53I and CaM-A102V, resulting in a reduced frequency for A102V. Therefore, the CPVT-associated CaM variants N53I and A102V not only increase the RyR2

P*o* but also cause changes in Ca^{2+} release dynamics at a global cellular level which will contribute to the arrhythmia phenotype.
We did not observe any significant effect of the CaM mutations on intracellular Ca^{2+} concentrations and non-RyR associated Ca^{2+} response (carbachol or thapsigargin) suggesting that CaM effects on Ca^{2+} signalling are essentially RyR2-mediated.

The CaM N53I variant has been identified in a large Swedish family where the mutation has been carried over for generations (Nyegaard et al., 2012). It represents the largest cohort of patients living with an arrhythmia-associated CaM mutation, which suggests that CaM N53I has a less severe clinical phenotype than other *de novo* CaM variants such as CaM A102V. This observation correlates with our data which showed a more pronounced dysregulation of Ca^{2+} signalling pathways for CaM A102V.

In summary, both CPVT-associated variants CaM-N53I and CaM-A102V affect CaM:RyR2 structure-function relationship resulting in Ca^{2+} release from SR, via unique molecular mechanisms. Based on our findings we propose that CaM-N53I likely acts through a loss of direct inhibition of RyR2 (subtle alterations in local structures), whereas for the CaM-A102V mutant, there is a finely tuned balance between loss of direct inhibition of RyR2 (higher K_d) and increased channel activation via CaMKIIδ phosphorylation (Fig. 7). The loss of inhibition and over-activation of RyR2 triggers abnormal Ca^{2+} release from the SR. The subsequent increase in cytoplasmic Ca^{2+} concentration would then promote anomalous cardiac muscle contractions and generate irregular heartbeats, characteristics of CPVT syndrome. Interestingly, our data demonstrate a potential role of CaMKIIδ in the molecular aetiology of the disease which could open ways for new therapeutic avenues.

Materials and Methods

Plasmids. For recombinant protein expression, the human CaM gene was subcloned from the pGEX-6P-1 vector (Lian et al., 2014) into pE-SUMOPro by restriction-ligation (BsaI/XbaI) using 5'-CAGGTCTCAAGGTATGGCTGACCAACTGACTG-3' and 5'-CATCTAGATTATCACTTTGCTGTCATCATTTG-3'. A series of site directed mutagenesis reactions were performed following the QuikChange protocol (Agilent Technologies) to generate CPVT-associated CaM constructs. Primers used were as follows: N53I; 5'-AGCAGAGTTACAGGACATGATTATTGAAGTAGATGCTGATG-3', A102V; 5'-GCAATGGCTATATTAGTGTTGCAGAACTTCGCCATGT-3'.
For the Ca^{2+} imaging experiments, CaM genes were subcloned from pE-SUMOPro into pHIV-dTomato (Addgene plasmid #21374) vectors by Gibson Assembly (NEBuilder) following the manufacturer recommendations and the NEBuilder assembly tool website. In these constructs, the IRES sequence allows CaM and dTomato to be co-expressed under the control of same promoter as two distinct proteins.
All resulting vectors were confirmed by DNA sequencing (DNA sequencing and Services, University of Dundee).
The molecular construct for expressing the human RyR2 (pcDNA-3/eGFP-hRyR2) was a kind gift from Dr Chris George (Swansea University Medical School). pHIV-dTomato was a gift from Bryan Welm (Addgene plasmid #21374).

Peptides. To circumvent the technical challenges associated with the production and use of full-length RyR2, we used two synthetic peptides (short and long) encompassing the calmodulin binding domain (CaMBD) for our biophysical experiments: $RyR2_{3583-3603}$

(KKAVWHKLLSKQRKRAVVACF) and $RyR2_{3581-3608}$ (RSKKAVWHKLLSKQRKRAVVACFRMAP). It has been shown that the deletion of residues 3583-3603 abolishes the interaction between CaM and RyR2 (Tian et al., 2013; Yamaguchi et al., 2003), suggesting that this domain is essential for CaM binding. In addition, a recent cryo-EM structure of CaM in complex with RyR2 confirmed that residues 3593–3607 in the central domain represents the primary interface with CaM (Gong et al., 2019).
The RyR2 peptides were synthesised and HPLC-purified by GenicBio (China) and purity was estimated as >95% through mass spectrometry.

Expression and purification of CaM proteins. Overexpression of CaM protein variants was performed in *E. coli* BL21(DE3) STAR. Cells were grown in 1L of 2xYT media (16 $g.L^{-1}$ tryptone, 10 $g.L^{-1}$ yeast extract and 5 $g.L^{-1}$ NaCl) at 37 °C, 200 rpm. Expression was induced by 0.5 mM isopropyl β-D-1-thiogalactopyranoside (IPTG) when OD_{600nm} reached 0.5-0.8, for 16-20h at 18 °C. Cells were resuspended in 50 mM Na^+-HEPES (pH 7.5), 200 mM NaCl, containing Proteoloc Protease Inhibitor Cocktail (Expedeon). Lysis was performed by incubation with 1 $mg.mL^{-1}$ lysozyme (Biozyme) on ice for 30 min followed by sonication (VibraCell, Jencons PLS). Lysates were then incubated with 500 Units of BaseMuncher endonuclease (Expedeon) to hydrolyse RNA and DNA contaminants and clarified through ultra-centrifugation at 100,000 g. Protein-containing supernatant was purified on an AKTA Start (GE Healthcare) using a 5 mL HisTrap HP column (GE Healthcare) equilibrated with 50 mM Na^+-HEPES (pH 7.5), 200 mM NaCl. Bound proteins were eluted by a linear gradient 0-500 mM imidazole. The His-SUMO tag was cleaved from the protein by SUMO-protease added to a ratio of 2000:1 (protein-protease), for one hour at 30 °C. The untagged CaM proteins were further purified on a 5 mL HisTrap HP and recovered in the flow through. The final step of purification was performed on an AKTA Pure (GE Healthcare) equipped with a Superdex 75 (16/600) size exclusion column (GE Healthcare) equilibrated with 20 mM Na^+-HEPES (pH 7.5), 50 mM NaCl.
For NMR measurements, *E. coli* BL21(DE3) STAR cultures producing uniformly isotopic labelled protein were grown in minimal media, containing 88 mM Na_2HPO_4, 55 mM KH_2PO_4, 30 µM thiamine-HCl, 136 µM $CaCl_2{\cdot}2H_2O$, 1 mM $MgSO_4{\cdot}7H_2O$, 19 mM $^{15}NH_4Cl$ and 22 mM glucose (or ^{13}C glucose for triple resonance NMR experiments). Overexpression and purification were performed as described above. Isotopically labelled reagents were purchased from Cambridge Isotope Laboratories.
Unlabelled and isotopically labelled protein purity was determined by SDS-PAGE (NuPAGE 4-12% Bis-Tris, Life Technologies) and relevant fractions were concentrated using an Amicon Ultra-15 centrifugation units (Millipore) with a 3 kDa cut-off. Purified proteins were aliquoted, flash-frozen in liquid nitrogen and stored at -80 °C.

Protein concentration measurements. Protein and peptide concentrations were measured by spectrophotometry at 280 nm (Nanodrop, Thermo Scientific) using ε_0 (CaM) = 2,980 $M^{-1}.cm^{-1}$, ε_0 (SUMO-protease) = 1,490 $M^{-1}.cm^{-1}$ and ε_0 (RyR2 peptides) = 5,500 $M^{-1}.cm^{-1}$.
Molar extinction coefficients were calculated from the amino acid composition using ExPASy/ProtParam program (Gasteiger et al., 2005).

Isothermal Titration Calorimetry (ITC). Experiments were performed in assay buffer (50 mM Na^+-HEPES, 100 mM KCl, 2 mM $MgCl_2$, pH 7.5) supplemented with either 5 mM $CaCl_2$ or 5 mM EGTA for Ca^{2+} dependent or independent binding events, respectively. EGTA was prepared as a stock solution (0.5 M with pH adjusted to pH 7.5 with KOH) and then added to the assay buffer (5 mM final) to prevent any final pH changes.

$RyR2_{3583-3603}$ and $RyR2_{3581-3608}$ peptides were titrated against CaM proteins across 20 injections (2 µL each) lasting four seconds with a 180 second grace period in-between. Peptide was typically titrated into the cell at a 10-fold higher concentration than CaM. CaM concentrations used were 10-45 µM in $CaCl_2$ and 140-180 µM in EGTA.
All titrations were performed using a MicroCal iTC200 and automated PEAQ-ITC systems (Malvern) at 25 °C under continuous stirring at 800 rpm. Data were processed using the MicroCal PEAQ-ITC software and fitted according to a one-site binding model.

Secondary structure determination of CaM proteins. Circular dichroism (CD) spectra were recorded using a JASCO J-1100 spectrometer equipped with a JASCO MCB-100 mini circulation bath for temperature control. Far-UV CD spectra (180-260 nm) were recorded at 20 °C in a 0.1 cm path length quartz cell (5 spectra accumulations, scan rate 50 $nm.min^{-1}$). Proteins (5 µM) were measured in 1 mM $CaCl_2$ or 1 mM EGTA. Secondary structure content was determined using CDSSTR prediction algorithm (DichroWeb online server, reference set3) (Johnson, 1999; Whitmore and Wallace, 2004; Whitmore and Wallace, 2008).

Protein susceptibility to protease degradation. Purified CaM (5 µM) was incubated with increasing concentrations of AspN endoproteinase (New England Biolabs) ranging from 0 to 300 $\mu g.mL^{-1}$ diluted in AspN-reaction buffer consisting of 50 mM Tris-HCl (pH 8.0), 2.5 mM $ZnSO_4$. Enzymatic reactions were incubated at 37 °C for 30 minutes either in the presence of 5 mM $CaCl_2$ or 5 mM EGTA, ± $RyR2_{3583-3603}$ peptide (12 µM). The amount of intact protein was assessed by SDS-PAGE (NuPAGE 4–12% Bis-Tris, Life Technologies) and Coomassie staining (InstantBlue, ThermoFisher). Images were taken using a ChemiDoc XRS+ transilluminator (Bio-Rad) and quantified by densitometry using Fiji software (Schindelin et al., 2012).

Protein thermal stability. Thermal stability of CaM proteins was determined by following the unfolding of the α-helices at 222 nm using circular dichroism (JASCO J-1100 CD spectrometer equipped with a JASCO MCB-100 mini circulation bath for temperature control, 200 µL quartz cuvette, 0.1 cm path length). Data were collected in 2 mM Na^+-HEPES buffer containing 1 mM EGTA and 10 µM CaM, from 15 to 80 °C using 300 sec equilibration time, 1 °C increment (1 $°C.min^{-1}$) and 3 accumulations. Signal recorded at each temperature was normalised as fraction of total signal change and subjected to Boltzmann sigmoid analysis to obtain melting point (T_m).

NMR Spectroscopy. All NMR spectra were collected at 30 °C (303 K) on an Avance III 800 MHz spectrometer equipped with [^1H, ^{15}N, ^{13}C]-cryoprobes (Bruker). ^1H-^{15}N Heteronuclear single quantum coherence (HSQC) experiments consisted of titrations of ^{15}N-labelled CaM variants (100 µM) with unlabelled RyR2 peptide. Peptide titrations were performed in 20 mM Na^+-HEPES (pH 7.5), 50 mM NaCl, 1 mM $CaCl_2$, 10% (v/v) D_2O, with the stepwise addition of $RyR2_{3583-3603}$ peptide to the protein sample after each recording to achieve 0.5:1, 1:1, 2:1 and 4:1 peptide:protein molar ratio. For chemical shift perturbation analysis, raw data were processed using the Bruker TopSpin software. Resonance peaks were analysed and assigned using CcpNmr software (Vranken et al., 2005).
Backbone amino-acid assignments for CaM variants were transferred from previously published solution NMR structures (BMRB entry 6541) (Kainosho et al., 2006). Ambiguous peaks were assigned using standard triple resonance experiments CBCA(CO)NH and CBCANH obtained using 1 mM ^{13}C-^{15}N CaM-WT. Chemical shift differences were expressed in ppm as $\Delta\delta = [(\Delta H)^2 + (0.15\Delta N)^2]^{1/2}$. Residues with chemical shifts equal to or less than 0.03 ppm were deemed non-movers, the remaining shifts were categorised into

colour by increasing margins of 0.03 ppm and mapped onto the structure of Ca^{2+}/CaM using PyMOL to illustrate a surface representation of the chemical shift derivations.

X-ray crystallography. Crystals for Ca^{2+}/CaM-WT:$RyR2_{3583-3603}$, Ca^{2+}/CaM-N53I:$RyR2_{3583-3603}$ and Ca^{2+}/CaM-A102V:$RyR2_{3583-3603}$ proteins were grown at 20 °C using the sitting drop vapour diffusion method (1 mM CaM, 1 mM $CaCl_2$, 1.2 mM $RyR2_{3583-3603}$ peptide). Ca^{2+}/CaM-WT:$RyR2_{3583-3603}$ crystallised in 0.1 M sodium acetate pH 4.5, 0.2 M ammonium acetate, 10% (w/v) PEG 4,000. Ca^{2+}/CaM-N53I:$RyR2_{3583-3603}$ crystallised in 0.1 M sodium acetate trihydrate pH 4.5, 10% (w/v) PEG 10,000. Ca^{2+}/CaM-A102V:$RyR2_{3583-3603}$ crystallised in 0.1 M sodium acetate trihydrate pH 4.0, 25% (w/v) PEG 1,500.
Crystals were cryo-protected using 20% (w/v) PEG 400 and diffraction data were collected at Diamond synchrotron beamline I03 (CaM-N53I and CaM-A102V) and SOLEIL Proxima 1 (CaM-WT). Data were processed by xia2/DIALS (Winter et al., 2018) and scaled by AIMLESS (Evans, 2006). Structure for wild-type protein was solved by molecular replacement with MOLREP (Vagin and Teplyakov, 2010), using Ca^{2+}/CaM-WT:$RyR1_{3614-3643}$ (PDB 2BCX) as a search model (Maximciuc et al., 2006). Structures of variants were refined starting from the wild-type structure using REFMAC5 (Murshudov et al., 1997) in the CCP4 programme suite (Potterton et al., 2003; Winn et al., 2011). Final steps of refinement for Ca^{2+}/CaM-WT:$RyR2_{3583-3603}$ were performed with anisotropic B-factors and hydrogens. Rebuilding of the model between refinement cycles and adding water molecules was performed in COOT (Emsley and Cowtan, 2004). The quality of the models was assessed on MolProbity server (Chen et al., 2010).
Summary of diffraction data, refinement statistics and the quality indicators for the structures are given in Table S2. PDB codes are 6XXF (Ca^{2+}/CaM-WT:$RyR2_{3583-3603}$), 6XY3 (Ca^{2+}/CaM-N53I:$RyR2_{3583-3603}$) and 6XXX (Ca^{2+}/CaM-A102V:$RyR2_{3583-3603}$).

CaMKIIδ phosphorylation activity measurements. Six-week-old male CD1 mice (Charles River) were humanely sacrificed by cervical dislocation (schedule 1 procedure) in accordance with the Animals (Scientific Procedures) Act (1986) under Establishment License 40/2408 and with approval by the University of Liverpool Animal Welfare Committee and Ethical Review Body. Mice hearts were surgically removed and homogenised with a blender in 3 mL of extraction buffer (20 mM Tris pH 8.0, 2 mM EDTA, 2 mM EGTA, 2 mM DTT, complete protease inhibitor ULTRA mini). Heart lysates were clarified by centrifugation and used as CaMKIIδ source for the assay. CaMKIIδ phosphorylation activity was determined using [γ^{32}P] ATP (Perkin Elmer) and the SignaTECT Calcium/ Calmodulin-Dependent Protein Kinase Assay System (Promega) according to the manufacturer's recommendation. Purified CaM and CPVT-associated mutant recombinant proteins were added in the reaction mix (1 µM) to determine the effect of disease-associated CaM variants on CaMKIIδ phosphorylation activity. Scintillation levels were measured on a Tri-Carb 2910 TR low activity liquid scintillation analyzer (Perkin Elmer).

Time course of CaMKIIδ autophosphorylation
300 nM GST-CaMKIIδ (Abcam, ab84552) and 1 µM calmodulin, were incubated in 50 mM K^+-HEPES, pH 7.5, 100 mM KCl, 2 mM $MgCl_2$, 5 mM 1,4-dithiothreitol (DTT), 100 µM $CaCl_2$ at room temperature. The reaction was started by adding 300 µM ATP and was terminated using SDS-containing Laemmli sample buffer at predefined time points (0, 15 s, 30 s, 60 s, 120 s and 300 s). Post separation of proteins by SDS-PAGE (NuPage™ 4-12% Bis-Tris), proteins were electro-transferred from the gel to a nitrocellulose membrane using iBlot™ 2 gel transfer device (7 minutes protocol consisting of 3 steps: 20V for 1 min, 23V for 4 min and 25V for 2 min). The membranes were blocked with 5% (w/v) fat-free

powdered milk in 0.1% (v/v) Tween-20, 50 mM Tris-HCl (pH 7.6), 150 mM NaCl (T-TBS buffer). Membranes were then probed overnight at 4 °C with mouse anti-GST (Sigma-Aldrich, G1160) and rabbit anti-phospho T287 (Abcam, ab182647) monoclonal primary antibodies at 1/1000 and 1/500 dilutions respectively. Next, membranes were washed in T-TBS and incubated for 1 hour at room temperature with IRDye® 680RD donkey anti-mouse (LI-COR, 926-68072) and IRDye® 800CW donkey anti-rabbit (LI-COR, 926-32213) IgG secondary antibodies at 1/10000 dilution. The bands were visualized using an Odyssey CLx infrared imaging system and the intensity of the bands were quantified by densitometry using Fiji.

Cell culture, transfection and Ca^{2+} imaging. HEK293T cells (ATCC®, UK) (1 x 10^5) were seeded onto 35 mm poly-lysine treated glass-bottomed dishes (MatTek Corporation). Cells were co-transfected with eGFP-hRyR2 (pcDNA3) and CaM variants (dTomato) plasmids in an equal molar ratio using Effectene reagent (Qiagen), according to the manufacturer's instructions. Cells were imaged after 48 hours of expression and loading with 10 µM Calbryte 520 AM (AAT Bioquest). Imaging was carried out at 37 °C/5%CO_2 (OKO lab incubation chamber) with a 3i Marianas spinning-disk confocal microscope equipped with a Zeiss AxioObserver Z1, a 20x/0.8 Plan-Apochromat air objective and a 3i Laserstack as excitation light source (488 nm, for Calbryte/eGFP; 561 nm, for dTomato). Emitted light was collected through single bandpass filters (CSU- X filter wheel; Yokogawa, Tokyo, Japan) onto a complementary metal- oxide semiconductor (CMOS) camera (Orca Flash 4.0; Hamamatsu, Japan).
Cells were covered with Krebs buffer (200 µl, pH 7.4, containing 1.3 mM $CaCl_2$) and data acquired at a rate of approximately 5 frames per second using SlideBook v.6 software at 1024 x 1024 pixel resolution. Spontaneous Ca^{2+} oscillations and ER load (10 mM caffeine) were recorded from cells co-expressing RyR2 (eGFP) and CaM variants (dTomato). Non-RyR2-associated Ca^{2+} response was obtained after addition of 10 µM carbachol or 2 µM thapsigargin from cells expressing CaM variants (dTomato). Calbryte 520 fluorescence signals were measured from regions of interest outlining individual cells using Ilastik for segmentation and Fiji for the intensity recording within the segmented areas (Berg et al., 2019; Schindelin et al., 2012). Kinetic parameters of Ca^{2+} release were quantified using Analyse Spikes applet for MatLab (Dr Aled Jones, QMUL).
For intra-cellular Ca^{2+} measurements, HEK293T cells expressing CaM variants (dTomato) were loaded with 5 µM fura-2 AM for 1 hour at 37 °C. Cells were imaged on a Nikon Eclipse TE200 microscope equipped with a 20x/0.45 Plan Fluor air objective, 48h post-transfection. Cells were illuminated at 340 and 380 nm using a PTI monochromator (PTI, Birmingham, NJ, USA) and fluorescence emissions were captured above 520 nm using an Andor Zyla 4.2 sCMOS camera (Andor Technology, Belfast). Images were acquired using Winfluor 4.0 software (University of Strathclyde). Data were processed on Fiji (Schindelin et al., 2012) and expressed as the ratio of the 340:380 nm signals.

Data Analysis and Statistics. Results are expressed as mean ± SEM unless indicated otherwise. Experiments were performed at least in triplicates and analysed using the GraphPad Prism software package. Significance level was obtained using two-tailed unpaired Student *t*-test, one-way ANOVA or two-way ANOVA. P values are represented by stars (*$P < 0.05$, **$P < 0.01$, ***$P < 0.001$, ****$P < 0.0001$). Structure representations were done using the PyMOL Molecular Graphics System software (v2.0.7) and figures were generated using CorelDRAW 2019.

Acknowledgements
We thank the staff and management Diamond and SOLEIL synchrotrons for provision of the crystallographic facilities. We would like to thank Dr Chris George (Swansea University Medical School) for allowing use of the pcDNA3-eGFP-hRyR2 plasmid, Dr Aled Jones (QMUL) for the AnalyseSpikes software and Dr Richard Rainbow for the use his microscopy equipment for the Fura-2 experiments. We are grateful to Prof Alexei Tepikin and Dr Helen Tanton (University of Liverpool) for providing mice heart tissues. Prof Alan Morgan (University of Liverpool) is thanked for his comments on the manuscript.

Competing interests
None declared

Funding
This work was supported by British Heart Foundation Intermediate Basic Science Research Fellowship FS/17/56/32925 to N. H., The Company of Biologists Travelling Fellowship JCS-180802 to N. H. and British Heart Foundation project grant PG/16/92/32453 to N.L.T.

References

Ai, X., Curran, J. W., Shannon, T. R., Bers, D. M. and Pogwizd, S. M. (2005). Ca2+/calmodulin-dependent protein kinase modulates cardiac ryanodine receptor phosphorylation and sarcoplasmic reticulum Ca2+ leak in heart failure. *Circ Res* **97**, 1314-22.

Balshaw, D. M., Xu, L., Yamaguchi, N., Pasek, D. A. and Meissner, G. (2001). Calmodulin binding and inhibition of cardiac muscle calcium release channel (ryanodine receptor). *J Biol Chem* **276**, 20144-53.

Balshaw, D. M., Yamaguchi, N. and Meissner, G. (2002). Modulation of intracellular calcium-release channels by calmodulin. *J Membr Biol* **185**, 1-8.

Bardai, A., Berdowski, J., van der Werf, C., Blom, M. T., Ceelen, M., van Langen, I. M., Tijssen, J. G. P., Wilde, A. A. M., Koster, R. W. and Tan, H. L. (2011). Incidence, Causes, and Outcomes of Out-of-Hospital Cardiac Arrest in Children: A Comprehensive, Prospective, Population-Based Study in the Netherlands. *Journal of the American College of Cardiology* **57**, 1822-1828.

Behere, S. P. and Weindling, S. N. (2016). Catecholaminergic polymorphic ventricular tachycardia: An exciting new era. *Ann Pediatr Cardiol* **9**, 137-46.

Ben-Johny, M., Dick, I. E., Sang, L., Limpitikul, W. B., Kang, P. W., Niu, J., Banerjee, R., Yang, W., Babich, J. S., Issa, J. B. et al. (2015). Towards a Unified Theory of Calmodulin Regulation (Calmodulation) of Voltage-Gated Calcium and Sodium Channels. *Curr Mol Pharmacol* **8**, 188-205.

Ben-Johny, M. and Yue, D. T. (2014). Calmodulin regulation (calmodulation) of voltage-gated calcium channels. *J Gen Physiol* **143**, 679-92.

Berchtold, M. W., Zacharias, T., Kulej, K., Wang, K., Torggler, R., Jespersen, T., Chen, J. N., Larsen, M. R. and la Cour, J. M. (2016). The Arrhythmogenic Calmodulin Mutation D129G Dysregulates Cell Growth, Calmodulin-dependent Kinase II Activity, and Cardiac Function in Zebrafish. *J Biol Chem* **291**, 26636-26646.

Berg, S., Kutra, D., Kroeger, T., Straehle, C. N., Kausler, B. X., Haubold, C., Schiegg, M., Ales, J., Beier, T., Rudy, M. et al. (2019). ilastik: interactive machine learning for (bio)image analysis. *Nat Methods* **16**, 1226-1232.

Bootman, M. D., Berridge, M. J. and Roderick, H. L. (2002). Calcium signalling: more messengers, more channels, more complexity. *Curr Biol* **12**, R563-5.

Brohus, M., Sondergaard, M. T., Wayne Chen, S. R., van Petegem, F. and Overgaard, M. T. (2019). Ca(2+)-dependent calmodulin binding to cardiac ryanodine receptor (RyR2) calmodulin-binding domains. *Biochem J* **476**, 193-209.

Chazin, W. J. and Johnson, C. N. (2020). Calmodulin Mutations Associated with Heart Arrhythmia: A Status Report. *Int J Mol Sci* **21**.

Chen, V. B., Arendall, W. B., 3rd, Headd, J. J., Keedy, D. A., Immormino, R. M., Kapral, G. J., Murray, L. W., Richardson, J. S. and Richardson, D. C. (2010). MolProbity: all-atom structure validation for macromolecular crystallography. *Acta Crystallogr D Biol Crystallogr* **66**, 12-21.

Dewenter, M., von der Lieth, A., Katus, H. A. and Backs, J. (2017). Calcium Signaling and Transcriptional Regulation in Cardiomyocytes. *Circ Res* **121**, 1000-1020.

Edman, C. F. and Schulman, H. (1994). Identification and characterization of delta B-CaM kinase and delta C-CaM kinase from rat heart, two new multifunctional Ca2+/calmodulin-dependent protein kinase isoforms. *Biochim Biophys Acta* **1221**, 89-101.

Eisenberg, D. (1984). Three-dimensional structure of membrane and surface proteins. *Annu Rev Biochem* **53**, 595-623.

Emsley, P. and Cowtan, K. (2004). Coot: model-building tools for molecular graphics. *Acta Crystallogr D Biol Crystallogr* **60**, 2126-32.

Endo, M. (1977). Calcium release from the sarcoplasmic reticulum. *Physiol Rev* **57**, 71-108.

Evans, P. (2006). Scaling and assessment of data quality. *Acta Crystallogr D Biol Crystallogr* **62**, 72-82.

Fischer, R., Koller, M., Flura, M., Mathews, S., Strehler-Page, M. A., Krebs, J., Penniston, J. T., Carafoli, E. and Strehler, E. E. (1988). Multiple divergent mRNAs code for a single human calmodulin. *J Biol Chem* **263**, 17055-62.

Gasteiger, E., Hoogland, C., Gattiker, A., Duvaud, S. e., Wilkins, M. R., Appel, R. D. and Bairoch, A. (2005). Protein Identification and Analysis Tools on the ExPASy Server. In *The Proteomics Protocols Handbook*, (ed. J. M. Walker), pp. 571-607. Totowa, NJ: Humana Press.

Gomez-Hurtado, N., Boczek, N. J., Kryshtal, D. O., Johnson, C. N., Sun, J., Nitu, F. R., Cornea, R. L., Chazin, W. J., Calvert, M. L., Tester, D. J. et al. (2016). Novel CPVT-Associated Calmodulin Mutation in CALM3 (CALM3-A103V) Activates Arrhythmogenic Ca Waves and Sparks. *Circ Arrhythm Electrophysiol* **9**.

Gong, D., Chi, X., Wei, J., Zhou, G., Huang, G., Zhang, L., Wang, R., Lei, J., Chen, S. R. W. and Yan, N. (2019). Modulation of cardiac ryanodine receptor 2 by calmodulin. *Nature* **572**, 347-351.

Hoch, B., Meyer, R., Hetzer, R., Krause, E. G. and Karczewski, P. (1999). Identification and expression of delta-isoforms of the multifunctional Ca2+/calmodulin-dependent protein kinase in failing and nonfailing human myocardium. *Circ Res* **84**, 713-21.

Hoeflich, K. P. and Ikura, M. (2002). Calmodulin in Action: Diversity in Target Recognition and Activation Mechanisms. *Cell* **108**, 739-742.

Holt, C., Hamborg, L., Lau, K., Brohus, M., Sorensen, A. B., Larsen, K. T., Sommer, C., Van Petegem, F., Overgaard, M. T. and Wimmer, R. (2020). The arrhythmogenic N53I variant subtly changes the structure and dynamics in the calmodulin N-terminal domain, altering its interaction with the cardiac ryanodine receptor. *J Biol Chem* **295**, 7620-7634.

Hudmon, A., Schulman, H., Kim, J., Maltez, J. M., Tsien, R. W. and Pitt, G. S. (2005). CaMKII tethers to L-type Ca2+ channels, establishing a local and dedicated integrator of Ca2+ signals for facilitation. *J Cell Biol* **171**, 537-47.

Hund, T. J. and Mohler, P. J. (2015). Role of CaMKII in cardiac arrhythmias. *Trends Cardiovasc Med* **25**, 392-7.

Hwang, H. S., Nitu, F. R., Yang, Y., Walweel, K., Pereira, L., Johnson, C. N., Faggioni, M., Chazin, W. J., Laver, D., George, A. L., Jr. et al. (2014). Divergent regulation of ryanodine receptor 2 calcium release channels by arrhythmogenic human calmodulin missense mutants. *Circ Res* **114**, 1114-24.

Jensen, H. H., Brohus, M., Nyegaard, M. and Overgaard, M. T. (2018). Human Calmodulin Mutations. *Front Mol Neurosci* **11**, 396.

Jiang, D., Xiao, B., Yang, D., Wang, R., Choi, P., Zhang, L., Cheng, H. and Chen, S. R. (2004). RyR2 mutations linked to ventricular tachycardia and sudden death reduce the threshold for store-overload-induced Ca2+ release (SOICR). *Proc Natl Acad Sci U S A* **101**, 13062-7.

Johnson, W. C. (1999). Analyzing protein circular dichroism spectra for accurate secondary structures. *Proteins* **35**, 307-12.

Kainosho, M., Torizawa, T., Iwashita, Y., Terauchi, T., Mei Ono, A. and Guntert, P. (2006). Optimal isotope labelling for NMR protein structure determinations. *Nature* **440**, 52-7.

Kim, J., Ghosh, S., Nunziato, D. A. and Pitt, G. S. (2004). Identification of the components controlling inactivation of voltage-gated Ca2+ channels. *Neuron* **41**, 745-54.

Krissinel, E. and Henrick, K. (2007). Inference of macromolecular assemblies from crystalline state. *J Mol Biol* **372**, 774-97.

Landstrom, A. P., Dobrev, D. and Wehrens, X. H. T. (2017). Calcium Signaling and Cardiac Arrhythmias. *Circ Res* **120**, 1969-1993.

Lanner, J. T., Georgiou, D. K., Joshi, A. D. and Hamilton, S. L. (2010). Ryanodine Receptors: Structure, Expression, Molecular Details, and Function in Calcium Release. *Cold Spring Harbor Perspectives in Biology* **2**, a003996.

Lau, K., Chan, M. M. and Van Petegem, F. (2014). Lobe-specific calmodulin binding to different ryanodine receptor isoforms. *Biochemistry* **53**, 932-46.

Lian, L. Y., Pandalaneni, S. R., Todd, P. A., Martin, V. M., Burgoyne, R. D. and Haynes, L. P. (2014). Demonstration of binding of neuronal calcium sensor-1 to the cav2.1 p/q-type calcium channel. *Biochemistry* **53**, 6052-62.

Linse, S., Helmersson, A. and Forsen, S. (1991). Calcium binding to calmodulin and its globular domains. *J Biol Chem* **266**, 8050-4.

Liu, N., Ruan, Y., Denegri, M., Bachetti, T., Li, Y., Colombi, B., Napolitano, C., Coetzee, W. A. and Priori, S. G. (2011). Calmodulin kinase II inhibition prevents arrhythmias in RyR2(R4496C+/-) mice with catecholaminergic polymorphic ventricular tachycardia. *J Mol Cell Cardiol* **50**, 214-22.

Liu, Y., Wei, J., Wong King Yuen, S. M., Sun, B., Tang, Y., Wang, R., Van Petegem, F. and Chen, S. R. W. (2017). CPVT-associated cardiac ryanodine receptor mutation G357S with reduced penetrance impairs Ca2+ release termination and diminishes protein expression. *PLoS One* **12**, e0184177.

Lucic, V., Greif, G. J. and Kennedy, M. B. (2008). Detailed state model of CaMKII activation and autophosphorylation. *Eur Biophys J* **38**, 83-98.

Luo, M. and Anderson, M. E. (2013). Mechanisms of Altered Ca2+ Handling in Heart Failure. *Circulation Research* **113**, 690-708.

Makita, N., Yagihara, N., Crotti, L., Johnson, C. N., Beckmann, B. M., Roh, M. S., Shigemizu, D., Lichtner, P., Ishikawa, T., Aiba, T. et al. (2014). Novel calmodulin mutations associated with congenital arrhythmia susceptibility. *Circ Cardiovasc Genet* **7**, 466-74.

Maximciuc, A. A., Putkey, J. A., Shamoo, Y. and Mackenzie, K. R. (2006). Complex of calmodulin with a ryanodine receptor target reveals a novel, flexible binding mode. *Structure* **14**, 1547-56.

Meyer, L., Stubbs, B., Fahrenbruch, C., Maeda, C., Harmon, K., Eisenberg, M. and Drezner, J. (2012). Incidence, Causes, and Survival Trends From Cardiovascular-Related Sudden Cardiac Arrest in Children and Young Adults 0 to 35 Years of Age: A 30-Year Review. *Circulation* **126**, 1363-1372.

Murshudov, G. N., Vagin, A. A. and Dodson, E. J. (1997). Refinement of macromolecular structures by the maximum-likelihood method. *Acta Crystallogr D Biol Crystallogr* **53**, 240-55.

Nyegaard, M., Overgaard, M. T., Sondergaard, M. T., Vranas, M., Behr, E. R., Hildebrandt, L. L., Lund, J., Hedley, P. L., Camm, A. J., Wettrell, G. et al. (2012). Mutations in calmodulin cause ventricular tachycardia and sudden cardiac death. *Am J Hum Genet* **91**, 703-12.

Pitt, G. S., Zuhlke, R. D., Hudmon, A., Schulman, H., Reuter, H. and Tsien, R. W. (2001). Molecular basis of calmodulin tethering and Ca2+-dependent inactivation of L-type Ca2+ channels. *J Biol Chem* **276**, 30794-802.

Potterton, E., Briggs, P., Turkenburg, M. and Dodson, E. (2003). A graphical user interface to the CCP4 program suite. *Acta Crystallogr D Biol Crystallogr* **59**, 1131-7.

Priori, S. G., Napolitano, C., Tiso, N., Memmi, M., Vignati, G., Bloise, R., Sorrentino, V. and Danieli, G. A. (2001). Mutations in the cardiac ryanodine receptor gene (hRyR2) underlie catecholaminergic polymorphic ventricular tachycardia. *Circulation* **103**, 196-200.

Rodriguez, P., Bhogal, M. S. and Colyer, J. (2003). Stoichiometric phosphorylation of cardiac ryanodine receptor on serine 2809 by calmodulin-dependent kinase II and protein kinase A. *J Biol Chem* **278**, 38593-600.

Schindelin, J., Arganda-Carreras, I., Frise, E., Kaynig, V., Longair, M., Pietzsch, T., Preibisch, S., Rueden, C., Saalfeld, S., Schmid, B. et al. (2012). Fiji: an open-source platform for biological-image analysis. *Nat Methods* **9**, 676-82.

Shifman, J. M., Choi, M. H., Mihalas, S., Mayo, S. L. and Kennedy, M. B. (2006). Ca2+/calmodulin-dependent protein kinase II (CaMKII) is activated by calmodulin with two bound calciums. *Proc Natl Acad Sci U S A* **103**, 13968-73.

Sigalas, C., Mayo-Martin, M. B., Jane, D. E. and Sitsapesan, R. (2009). Ca2+-calmodulin increases RyR2 open probability yet reduces ryanoid association with RyR2. *Biophys J* **97**, 1907-16.

Sondergaard, M. T., Liu, Y., Brohus, M., Guo, W., Nani, A., Carvajal, C., Fill, M., Overgaard, M. T. and Chen, S. R. W. (2019). Diminished inhibition and facilitated activation of RyR2-mediated Ca(2+) release is a common defect of arrhythmogenic calmodulin mutations. *FEBS J* **286**, 4554-4578.

Sondergaard, M. T., Liu, Y., Larsen, K. T., Nani, A., Tian, X., Holt, C., Wang, R., Wimmer, R., Van Petegem, F., Fill, M. et al. (2016). The Arrhythmogenic Calmodulin p.Phe142Leu Mutation Impairs C-domain Ca2+-binding but not Calmodulin-dependent Inhibition of the Cardiac Ryanodine Receptor. *J Biol Chem*.

Sondergaard, M. T., Sorensen, A. B., Skov, L. L., Kjaer-Sorensen, K., Bauer, M. C., Nyegaard, M., Linse, S., Oxvig, C. and Overgaard, M. T. (2015a). Calmodulin mutations causing catecholaminergic polymorphic ventricular tachycardia confer opposing functional and biophysical molecular changes. *FEBS J* **282**, 803-16.

Sondergaard, M. T., Tian, X., Liu, Y., Wang, R., Chazin, W. J., Chen, S. R. and Overgaard, M. T. (2015b). Arrhythmogenic Calmodulin Mutations Affect the Activation and Termination of Cardiac Ryanodine Receptor-mediated Ca2+ Release. *J Biol Chem* **290**, 26151-62.

Tian, X., Tang, Y., Liu, Y., Wang, R. and Chen, S. R. (2013). Calmodulin modulates the termination threshold for cardiac ryanodine receptor-mediated Ca2+ release. *Biochem J* **455**, 367-75.

Toutenhoofd, S. L., Foletti, D., Wicki, R., Rhyner, J. A., Garcia, F., Tolon, R. and Strehler, E. E. (1998). Characterization of the human CALM2 calmodulin gene and comparison of the transcriptional activity of CALM1, CALM2 and CALM3. *Cell Calcium* **23**, 323-38.

Vagin, A. and Teplyakov, A. (2010). Molecular replacement with MOLREP. *Acta Crystallogr D Biol Crystallogr* **66**, 22-5.

Van Petegem, F. (2012). Ryanodine receptors: structure and function. *J Biol Chem* **287**, 31624-32.

Van Petegem, F., Chatelain, F. C. and Minor, D. L., Jr. (2005). Insights into voltage-gated calcium channel regulation from the structure of the CaV1.2 IQ domain-Ca2+/calmodulin complex. *Nat Struct Mol Biol* **12**, 1108-15.

Vassilakopoulou, V., Calver, B. L., Thanassoulas, A., Beck, K., Hu, H., Buntwal, L., Smith, A., Theodoridou, M., Kashir, J., Blayney, L. et al. (2015). Distinctive malfunctions of calmodulin mutations associated with heart RyR2-mediated arrhythmic disease. *Biochim Biophys Acta* **1850**, 2168-76.

Vranken, W. F., Boucher, W., Stevens, T. J., Fogh, R. H., Pajon, A., Llinas, M., Ulrich, E. L., Markley, J. L., Ionides, J. and Laue, E. D. (2005). The CCPN data model for NMR spectroscopy: development of a software pipeline. *Proteins* **59**, 687-96.

Walweel, K., Gomez-Hurtado, N., Rebbeck, R. T., Oo, Y. W., Beard, N. A., Molenaar, P., Dos Remedios, C., van Helden, D. F., Cornea, R. L., Knollmann, B. C. et al. (2019). Calmodulin inhibition of human RyR2 channels requires phosphorylation of RyR2-S2808 or RyR2-S2814. *J Mol Cell Cardiol* **130**, 96-106.

Walweel, K., Oo, Y. W. and Laver, D. R. (2017). The emerging role of calmodulin regulation of RyR2 in controlling heart rhythm, the progression of heart failure and the antiarrhythmic action of dantrolene. *Clin Exp Pharmacol Physiol* **44**, 135-142.

Wang, K., Brohus, M., Holt, C., Overgaard, M. T., Wimmer, R. and Van Petegem, F. (2020). Arrhythmia mutations in calmodulin can disrupt cooperativity of Ca(2+) binding and cause misfolding. *J Physiol* **598**, 1169-1186.

Wehrens, X. H., Lehnart, S. E. and Marks, A. R. (2005). Intracellular calcium release and cardiac disease. *Annu Rev Physiol* **67**, 69-98.

Wehrens, X. H., Lehnart, S. E., Reiken, S. R. and Marks, A. R. (2004). Ca2+/calmodulin-dependent protein kinase II phosphorylation regulates the cardiac ryanodine receptor. *Circ Res* **94**, e61-70.

Whitmore, L. and Wallace, B. A. (2004). DICHROWEB, an online server for protein secondary structure analyses from circular dichroism spectroscopic data. *Nucleic Acids Res* **32**, W668-73.

Whitmore, L. and Wallace, B. A. (2008). Protein secondary structure analyses from circular dichroism spectroscopy: methods and reference databases. *Biopolymers* **89**, 392-400.

Winn, M. D., Ballard, C. C., Cowtan, K. D., Dodson, E. J., Emsley, P., Evans, P. R., Keegan, R. M., Krissinel, E. B., Leslie, A. G., McCoy, A. et al. (2011). Overview of the CCP4 suite and current developments. *Acta Crystallogr D Biol Crystallogr* **67**, 235-42.

Winter, G., Waterman, D. G., Parkhurst, J. M., Brewster, A. S., Gildea, R. J., Gerstel, M., Fuentes-Montero, L., Vollmar, M., Michels-Clark, T., Young, I. D. et al. (2018). DIALS: implementation and evaluation of a new integration package. *Acta Crystallogr D Struct Biol* **74**, 85-97.

Witcher, D. R., Kovacs, R. J., Schulman, H., Cefali, D. C. and Jones, L. R. (1991). Unique phosphorylation site on the cardiac ryanodine receptor regulates calcium channel activity. *J Biol Chem* **266**, 11144-52.

Witcher, D. R., Strifler, B. A. and Jones, L. R. (1992). Cardiac-specific phosphorylation site for multifunctional Ca2+/calmodulin-dependent protein kinase is conserved in the brain ryanodine receptor. *J Biol Chem* **267**, 4963-7.

Xu, L. and Meissner, G. (2004). Mechanism of calmodulin inhibition of cardiac sarcoplasmic reticulum Ca2+ release channel (ryanodine receptor). *Biophys J* **86**, 797-804.

Yamaguchi, N., Chakraborty, A., Huang, T. Q., Xu, L., Gomez, A. C., Pasek, D. A. and Meissner, G. (2013). Cardiac hypertrophy associated with impaired regulation of cardiac ryanodine receptor by calmodulin and S100A1. *Am J Physiol Heart Circ Physiol* **305**, H86-94.

Yamaguchi, N., Takahashi, N., Xu, L., Smithies, O. and Meissner, G. (2007). Early cardiac hypertrophy in mice with impaired calmodulin regulation of cardiac muscle Ca release channel. *J Clin Invest* **117**, 1344-53.

Yamaguchi, N., Xu, L., Pasek, D. A., Evans, K. E. and Meissner, G. (2003). Molecular basis of calmodulin binding to cardiac muscle Ca(2+) release channel (ryanodine receptor). *J Biol Chem* **278**, 23480-6.

Yang, D., Song, L. S., Zhu, W. Z., Chakir, K., Wang, W., Wu, C., Wang, Y., Xiao, R. P., Chen, S. R. and Cheng, H. (2003). Calmodulin regulation of excitation-contraction coupling in cardiac myocytes. *Circ Res* **92**, 659-67.

Yang, Y., Guo, T., Oda, T., Chakraborty, A., Chen, L., Uchinoumi, H., Knowlton, A. A., Fruen, B. R., Cornea, R. L., Meissner, G. et al. (2014). Cardiac myocyte Z-line calmodulin is mainly RyR2-bound, and reduction is arrhythmogenic and occurs in heart failure. *Circ Res* **114**, 295-306.

Zhang, M., Abrams, C., Wang, L., Gizzi, A., He, L., Lin, R., Chen, Y., Loll, P. J., Pascal, J. M. and Zhang, J. F. (2012). Structural basis for calmodulin as a dynamic calcium sensor. *Structure* **20**, 911-23.

Zhao, Y. T., Valdivia, C. R., Gurrola, G. B., Powers, P. P., Willis, B. C., Moss, R. L., Jalife, J. and Valdivia, H. H. (2015). Arrhythmogenesis in a catecholaminergic polymorphic ventricular tachycardia mutation that depresses ryanodine receptor function. *Proc Natl Acad Sci U S A* **112**, E1669-77.

Figures

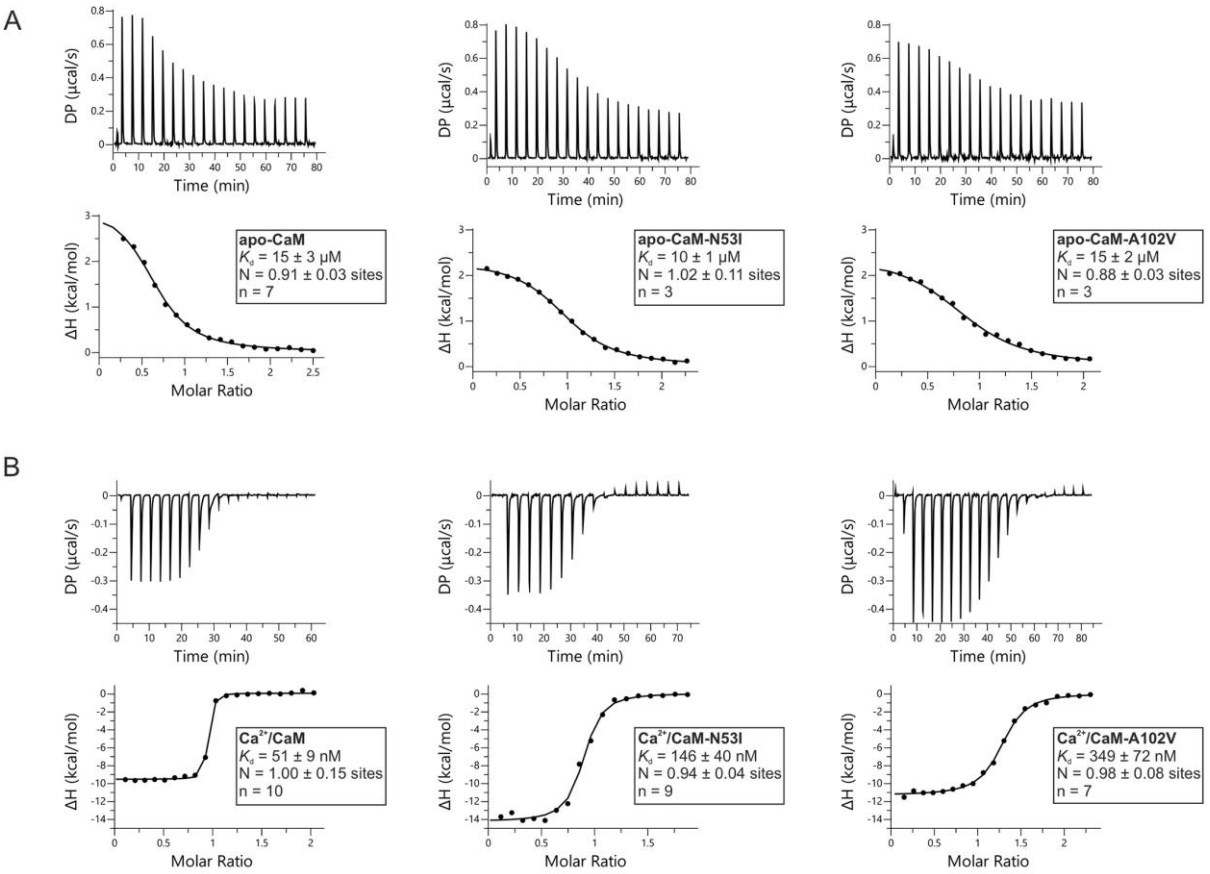

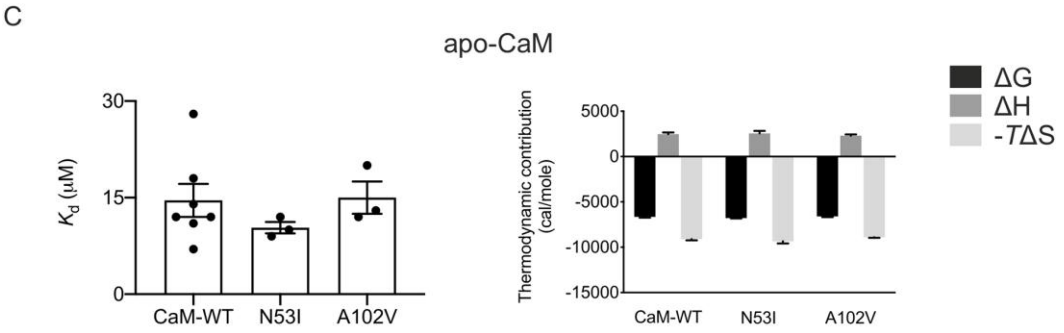

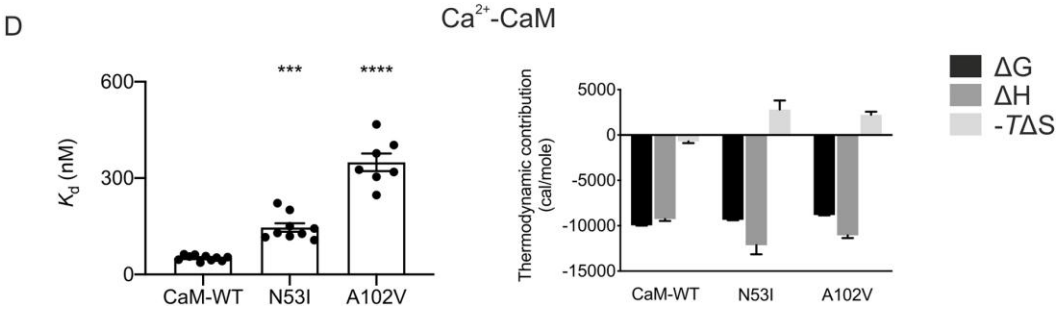

Figure 1. Ca^{2+}/CaM binding to RyR2 is decreased for the CPVT-associated variants N53I and A102V. Representative ITC titration curves (upper panel) and binding isotherms (lower panel) for CaM interaction with $RyR2_{3583-3603}$ in the (A) absence and (B) presence of Ca^{2+}. Affinity and thermodynamic profile of the binding of (C) apo-CaM and (D) Ca^{2+}/CaM proteins to $RyR2_{3583-3603}$ obtained by fitting to one-site binding model. Data were processed using the MicroCal PEAQ-ITC software. Data are expressed as mean ± SEM. N is for stoichiometry, n is the number of experimental replicates. The sum of the change in enthalpy (ΔH) and the change in entropy (ΔS) multiplied by the absolute temperature (T) gives the change in free energy (ΔG). Experiments were performed in the presence of 5 mM EGTA or 5 mM $CaCl_2$ at 25 °C. Number of replicates (n) for each conditions is shown on panel a and b. Differences between three groups were determined using one-way ANOVA with the Dunnett's post-hoc test. *$P < 0.05$, ****$P < 0.0001$, vs. CaM-WT.

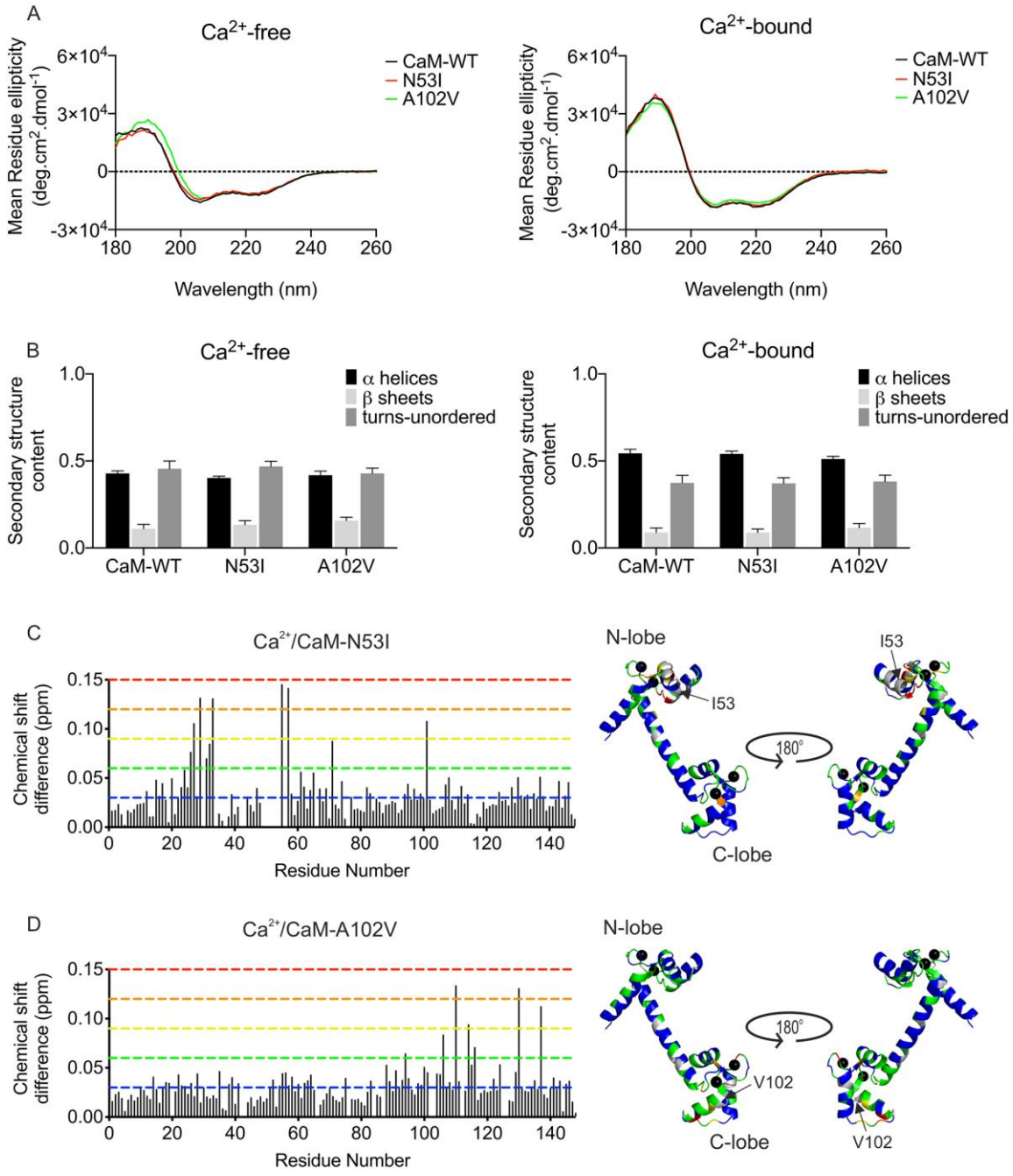

Figure 2. CPVT-associated CaM variants N53I and A102V do not show altered secondary structure but induce local structural changes in CaM. Analysis of the secondary structures of CaM-WT and mutants (5 μM) using circular dichroism (CD) spectroscopy. (A) CD spectra were obtained in the presence of 1 mM EGTA (left panel) or 1 mM $CaCl_2$ (right panel) and (B) protein secondary structure content estimated using CDSSTR method (Dichroweb, reference set3).

Data are expressed as mean ± SEM. Experiments were performed at 20 °C, in triplicate. Differences between three groups were determined using two-way ANOVA with the Sidak's post-hoc test and CaM-WT as control.

Histogram of chemical shift differences observed between CaM-WT and (C) CaM-N53I or (D) CaM-A102V (left panel). Chemical shift data were normalised between minimum and maximum values and converted into a colour spectrum of five unique colours (key, blue for smallest shifts through to red for largest shifts) which were then mapped onto the CaM

crystal structure (PDB 2CLL) (right panel). Unassigned peaks are shown in grey and Ca^{2+} ions in black spheres.

Chemical shift differences were expressed in ppm as $\Delta\delta = [(\Delta H)^2 + (0.15\Delta N)^2]^{1/2}$. Residues with chemical shifts equal to or less than 0.03 ppm were deemed non-movers (blue), the remaining shifts were categorised into colour by increasing margins of 0.03 ppm (0.03-0.06 ppm, green; 0.06-0.09 pm, yellow; 0.09-0.12pm, orange and 0.12-0.15 ppm, red). Shift differences were mapped onto the structure of Ca^{2+}/CaM using PyMOL to illustrate a surface representation of the chemical shift derivations.

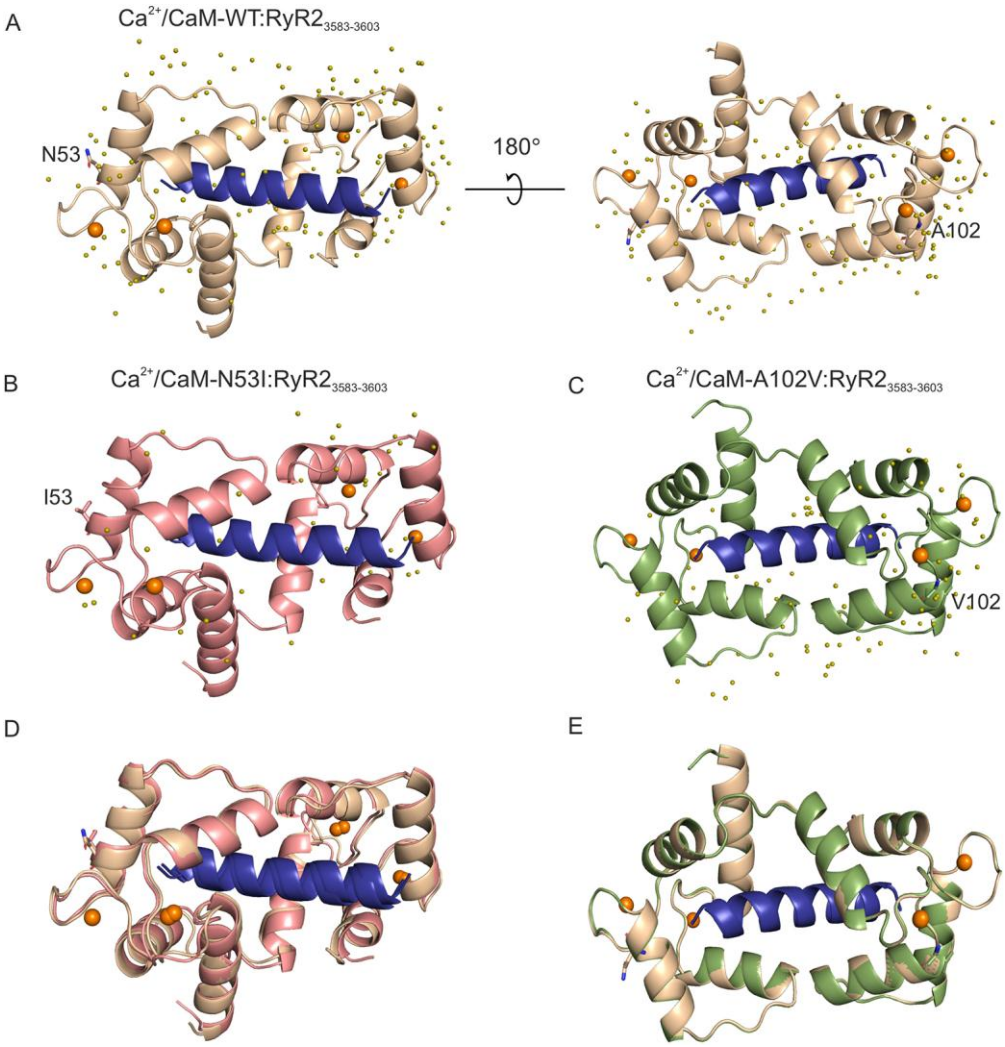

Figure 3. The arrhythmogenic N53I mutant causes subtle changes in the 3D structure of Ca^{2+}/CaM:$RyR2_{3583-3603}$. Cartoon representation of the crystal structures of Ca^{2+}/CaM proteins in complex with RyR2 peptide. (A) Ca^{2+}/CaM-WT:$RyR2_{3583-3603}$ (PDB 6XXF), (B) Ca^{2+}/CaM-N53I:$RyR2_{3583-3603}$ (PDB 6XY3), and (C) Ca^{2+}/CaM-A102V:$RyR2_{3583-3603}$ (PDB 6XXX). Alignment of Ca^{2+}/CaM-WT:$RyR2_{3583-3603}$ with (D) Ca^{2+}/CaM-N53I:$RyR2_{3583-3603}$, or (E) Ca^{2+}/CaM-A102V:$RyR2_{3583-3603}$ complex structures.
Ca^{2+} ions are shown in orange spheres and water molecules in olive spheres. The wild-type and mutant residues are shown in stick representation. CaM-WT is displayed in beige, CaM-N53I in salmon, CaM-A102V in green and $RyR2_{3583-3603}$ peptide in blue. Images were generated using PyMOL software.

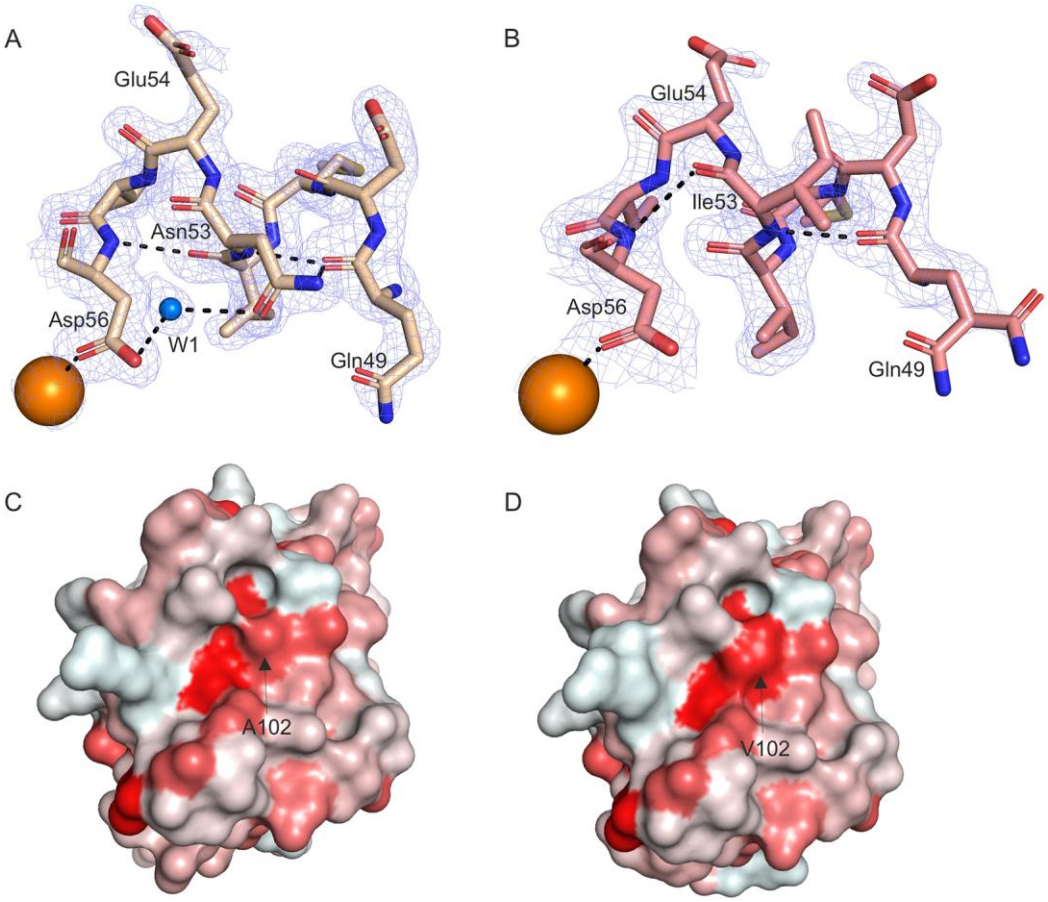

Figure 4. Ca^{2+}/CaM:RyR2$_{3583-3603}$ peptide complexes show differences in the H-bond network at the site of mutation and increased hydrophobicity. (A) Ca^{2+}/CaM-WT:RyR2$_{3583-3603}$ with Ca^{2+}/CaM-WT in beige and (B) Ca^{2+}/CaM-N53I:RyR2$_{3583-3603}$ with Ca^{2+}/CaM-N53I in salmon. Ca^{2+} ions are shown in orange spheres and water molecule in blue sphere. Interactions are represented in black dashed lines with residues represented in sticks and electron density in mesh.

Comparison of the hydrophobicity of the surface areas of (C) Ca^{2+}/CaM-WT:RyR2$_{3583-3603}$ and (D) Ca^{2+}/CaM-A102V:RyR2$_{3583-3603}$. CaM is shown in surface representation, with surface coloured from white to red based on Eisenberg hydrophobicity scale (Eisenberg, 1984). White is less hydrophobic than red. Arrow heads indicate the areas of the Ala102 and Val102 residues.

Images were generated using PyMOL software.

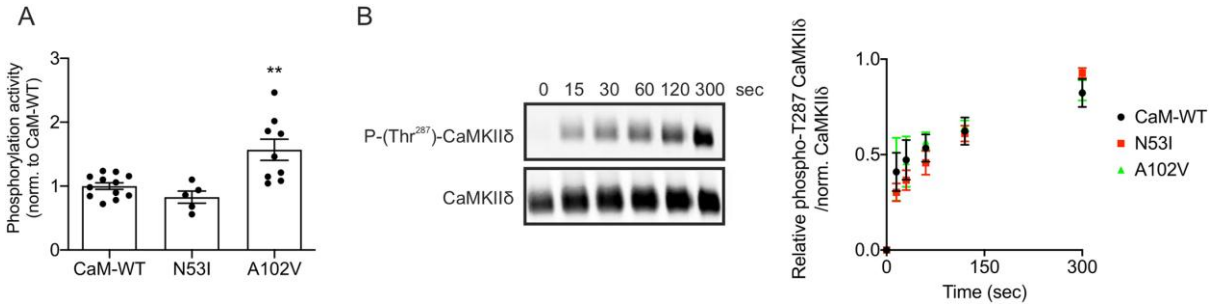

Figure 5. Arrhythmogenic variant A102V increases CaMKIIδ substrate phosphorylation activity while T287 CaMKIIδ autophosphorylation levels remain unchanged. (A) Quantification of phosphorylation activity of CaMKIIδ using radiolabelled ATP. CaMKIIδ activity measurements were performed using the SignaTECT Calcium/Calmodulin-Dependent Protein Kinase Assay System (Promega) on freshly isolated mice hearts. CaM-WT, CaM-N53I or CaM-A102V recombinant proteins (1 μM) were used as CaMKIIδ activators. [γ-^{32}P]-syntide-2 was used as an indicator of CaMKIIδ phosphorylation activity and quantified by scintillation counter. Data are expressed as mean ± SEM. Number of experimental replicates was: n=12 for CaM-WT, n=5 for CaM-N53I and n=9 for CaM-A102V, from 3 independent mice heart lysates preparations. Differences between three groups were determined using one-way ANOVA with the Dunnett's post-hoc test. **$P < 0.01$, vs. CaM-WT.

(B) Measurement of the relative levels of CaMKIIδ Thr^{287} autophosphorylation. GST-CaMKIIδ was incubated with calmodulin variants and ATP for 0, 15 s, 30 s, 60 s, 120 s and 300 s at room temperature. CaM-WT, CaM-N53I or CaM-A102V recombinant proteins were used as CaMKIIδ activators. The reaction was terminated using SDS-containing Laemmli buffer and samples were analysed by western blot and densitometry analysis. Phosphorylated proteins (phospho-Thr^{287} antibody) were normalized to total CaMKIIδ protein (GST antibody). Data are expressed as mean ± SEM. Number of experimental replicates was: n=4 for CaM-WT, n=3 for CaM-N53I and n=3 for CaM-A102V.

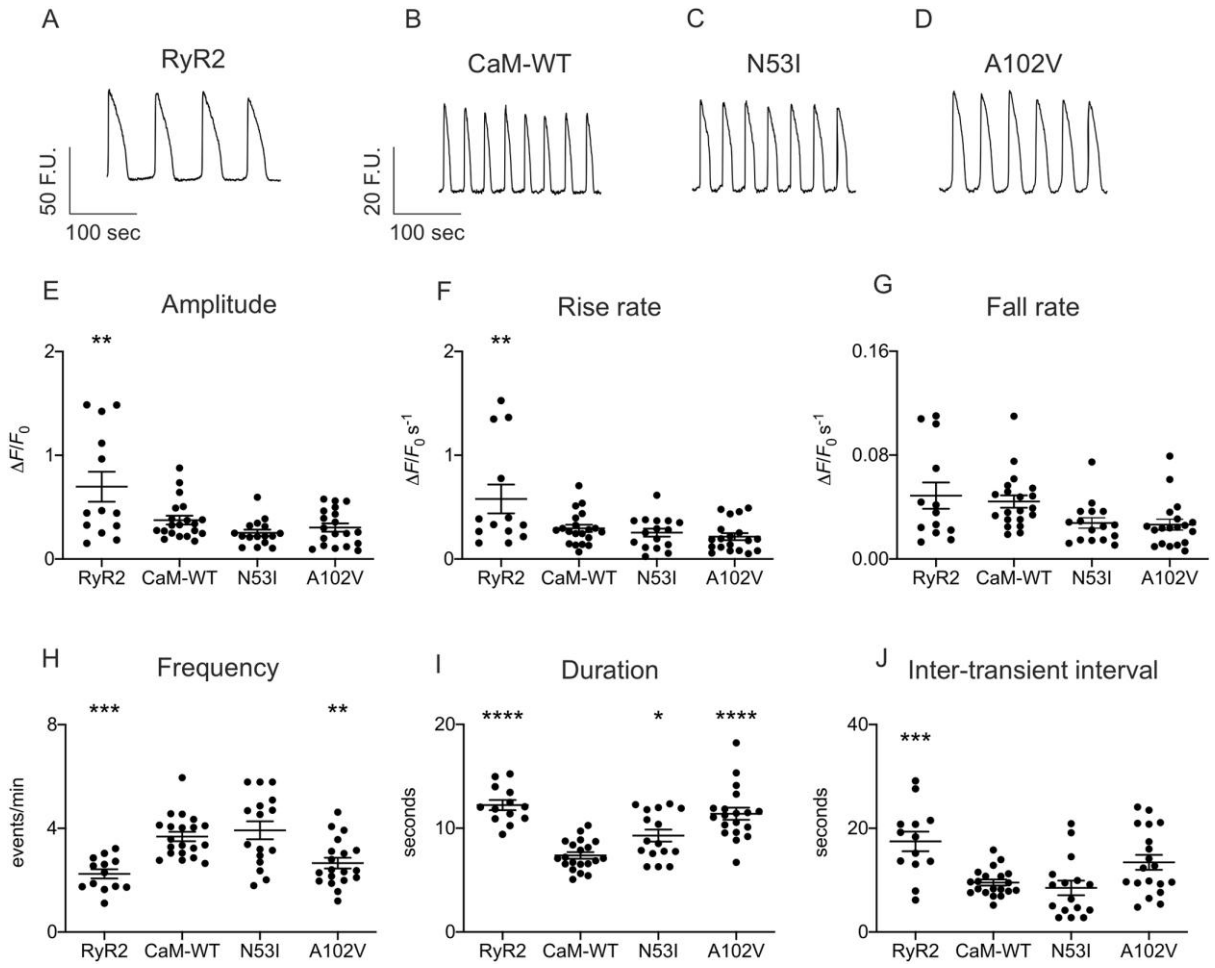

Figure 6. CPVT-associated mutations N53I and A102V affect spontaneous Ca^{2+} transients in cells. HEK293T cells transfected with RyR2 and CaM variants were loaded with Calbryte 520 to monitor intracellular Ca^{2+} concentration changes. Live cells were imaged on a 3i spinning-disk confocal microscope. Representative fluorescence signals HEK293T cells expressing (A) RyR2 with (B) CaM-WT, (C) CaM-N53I and (D) CaM-A102V. (E-J) Analysis of the Ca^{2+} transients kinetic parameters using Analyse Spikes applet for Matlab and Fiji (Schindelin et al., 2012), respectively. Data are expressed as mean ± SEM. Number of experimental replicates for the oscillations experiments (N=dishes, n=fields of view) was: N=6, n=20 for CaM-WT, N=6, n=16 for CaM-N53I and N=6, n=19 for CaM-A102V. Differences between groups were determined using one-way ANOVA with the Dunnett's post-hoc test. *$P < 0.05$, **$P < 0.01$ and ****$P < 0.0001$, vs. CaM-WT.

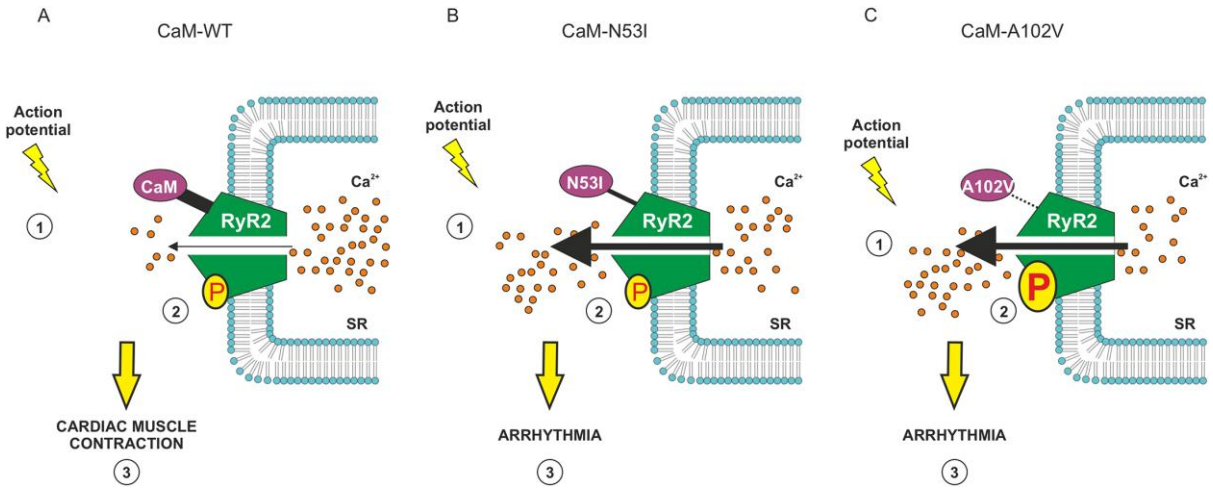

Figure 7. Proposed regulatory mechanisms for CPVT-associated CaM variants.
(1) Upon stimulation (action potential), Ca^{2+} enters the cell through L-type Ca^{2+} channels ($Ca_v1.2$) and (2) triggers release from the RyR2 by a process known as Ca^{2+}-induced Ca^{2+} release. (3) Cytosolic Ca^{2+} diffuses to myofibrils and promotes interaction between actin and myosin that leads to cardiac muscle contraction.
(A) In normal condition, Ca^{2+}/CaM modulates RyR2 activity through direct binding (inhibition) and phosphorylation via CaMKII (activation). A fine-tuned balance between these two processes is required to control cardiac muscle contraction.
(B) CaM-N53I: moderate reduction in affinity for RyR2 and altered CaM conformation reduce the inhibition of RyR2 by Ca^{2+}/CaM. This leads to an increase of Ca^{2+} release from the SR, promoting arrhythmia.
(C) CaM-A102V: large reduction in affinity for RyR2 reduces the inhibition of RyR2 by Ca^{2+}/CaM is combined with an increased CaMKIIδ phosphorylation activity, which promote the opening of the RyR2 channel. Both phenomena lead to an increase of Ca^{2+} release from the SR, promoting arrhythmia.

Table 1. Summary of biophysical properties of CPVT-associated CaM variants.

	K_d for $RyR2_{3583-3603}$ (apo) (+Ca^{2+})		**Tm (apo)**	**CaMKIIδ phosphorylation activity (fold change)**	**Ca^{2+} imaging in HEK293T**			
					Frequency (events/min)	Duration (seconds)	Inter-transient interval (seconds)	ER load ($\Delta F/F_0$)
CaM-WT	15 ± 3 μM	51 ± 9 nM	41.6 ± 0.3 °C	1.00 ± 0.05	3.7 ± 0.2	7.4 ± 0.3	9.5 ± 0.6	1.2 ± 0.2
N53I	10 ± 1 μM	146 ± 40 nM *	37.0 ± 0.7 °C ****	0.83 ± 0.10	3.9 ± 0.3	9.3 ± 0.6 *	8.5 ± 1.4	0.9 ± 0.2
A102V	15 ± 2 μM	349 ± 72 nM ****	39.3 ± 0.4 °C **	1.57 ± 0.17 **	2.7 ± 0.2 **	11.4 ± 0.6 ****	13.4 ± 1.4	0.9 ± 0.1

*P < 0.05, **P < 0.01, ****P < 0.0001, vs. CaM-WT

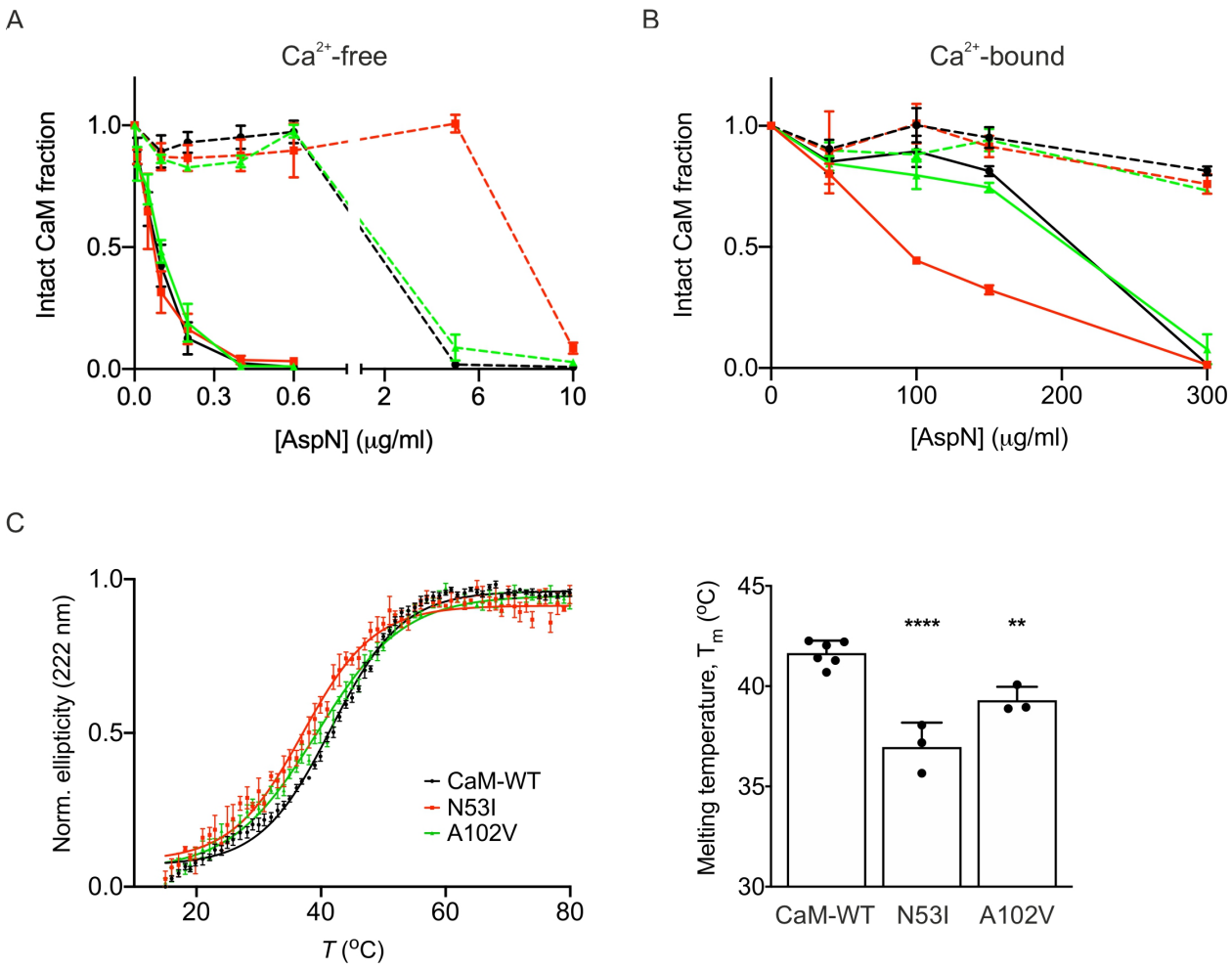

Fig. S1. Arrhythmogenic mutations N53I and A102V affect protease and thermal stability of CaM. (A-B) AspN limited proteolysis of CaM-WT and mutants in (A) absence and (B) presence of Ca^{2+}. Purified CaM proteins (CaM-WT, black; CaM-N53I, red; CaM-A102V, green) were mixed with increasing [AspN] for 30 minutes at 37 °C, with (dotted line) or without (plain lines) pre-incubation with $RyR2_{3583-3603}$ peptide. The fraction of intact CaM was determined by SDS-PAGE and Coomassie staining. Bands were quantified by densitometry analysis (Fiji). Data were normalised and expressed as mean ± SEM. Experiments were performed in 3-5 independent replicates.

Number of experimental replicates for apo-conditions was: n=4 for CaM-WT, n=4 for CaM-N53I, n=5 for CaM-A102V, n=4 for CaM-WT:RyR2, n=4 for CaM-N53I:RyR2 and n=4 for CaM-A102V:RyR2. Number of experimental replicates for Ca^{2+}-saturating conditions was: n=3 for CaM-WT, n=3 for CaM-N53I, n=3 for CaM-A102V, n=3 for CaM-WT:RyR2, n=3 for CaM-N53I:RyR2 and n=3 for CaM-A102V:RyR2.

(C) Thermal unfolding of CaM proteins (10 μM) monitored by circular dichroism recorded at 222 nm from 15 to 80 °C, in the presence of 1 mM EGTA. Data were normalised and expressed as mean ± SEM. Melting temperature (T_m) was obtained by fitting the traces to the Boltzmann equation. Number of experimental replicates was: n=6 for CaM-WT, n=3 for CaM-N53I and n=3 for CaM-A102V. Differences between three groups were determined using one-way ANOVA with the Dunnett's post-hoc test. **P < 0.01, ****P < 0.0001, vs. CaM-WT.

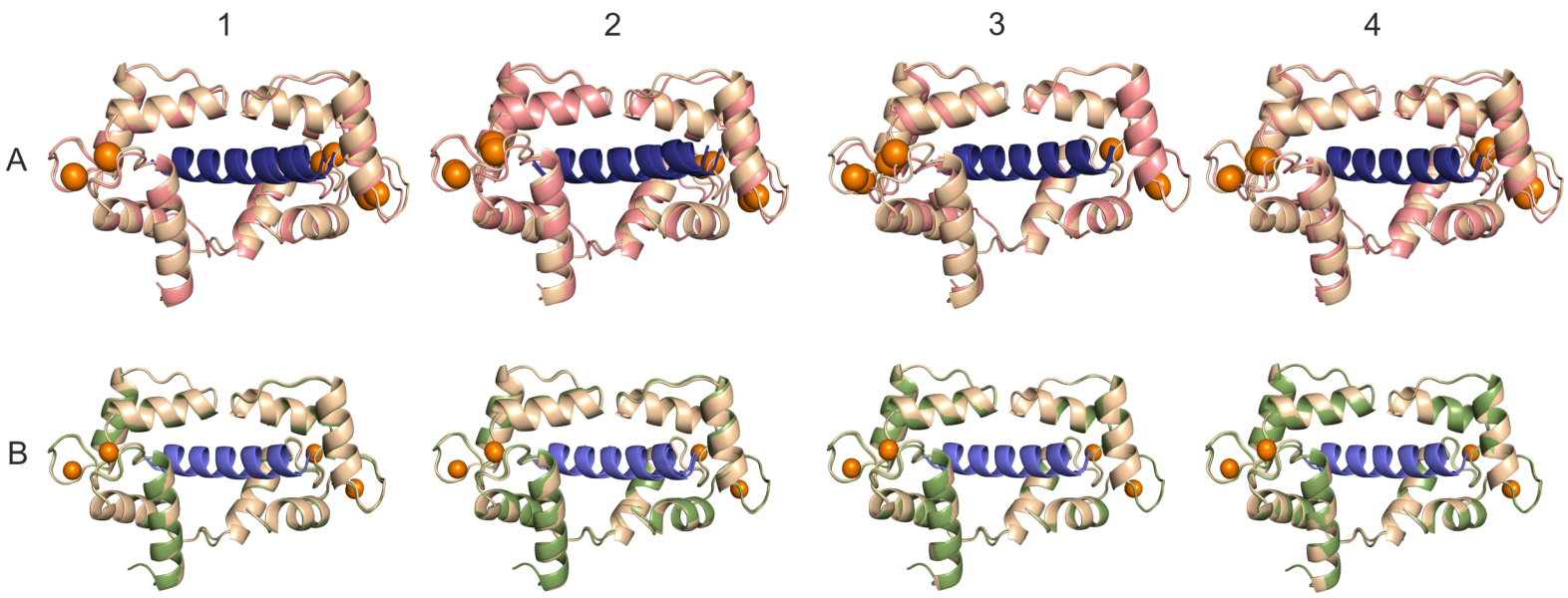

Fig. S2. Structural superposition of Cα atoms of Ca^{2+}/CaM-RyR peptide complexes. Superimposition of the crystal structure of Ca^{2+}/CaM-WT:$RyR2_{3583-3603}$ and (A) Ca^{2+}/CaM-N53I:$RyR2_{3583-3603}$ or (B) Ca^{2+}/CaM-A102V:$RyR2_{3583-3603}$. Superimposition was based on (1) N-terminal region (residues 5-64), (2) flexible helix region (residues 65-92), (3) C-terminal region (residues 93-148) or (4) RyR2 peptide.
CaM-WT is displayed in beige (CaM-WT from PDB 2BCX is displayed in yellow), CaM-N53I in salmon and CaM-A102V in green. $RyR2_{3583-3603}$ (KKAVWHKLLSKQRKRAVVACF) is shown in blue. Ca^{2+} ions are represented as orange spheres. Images were generated using PyMOL software.

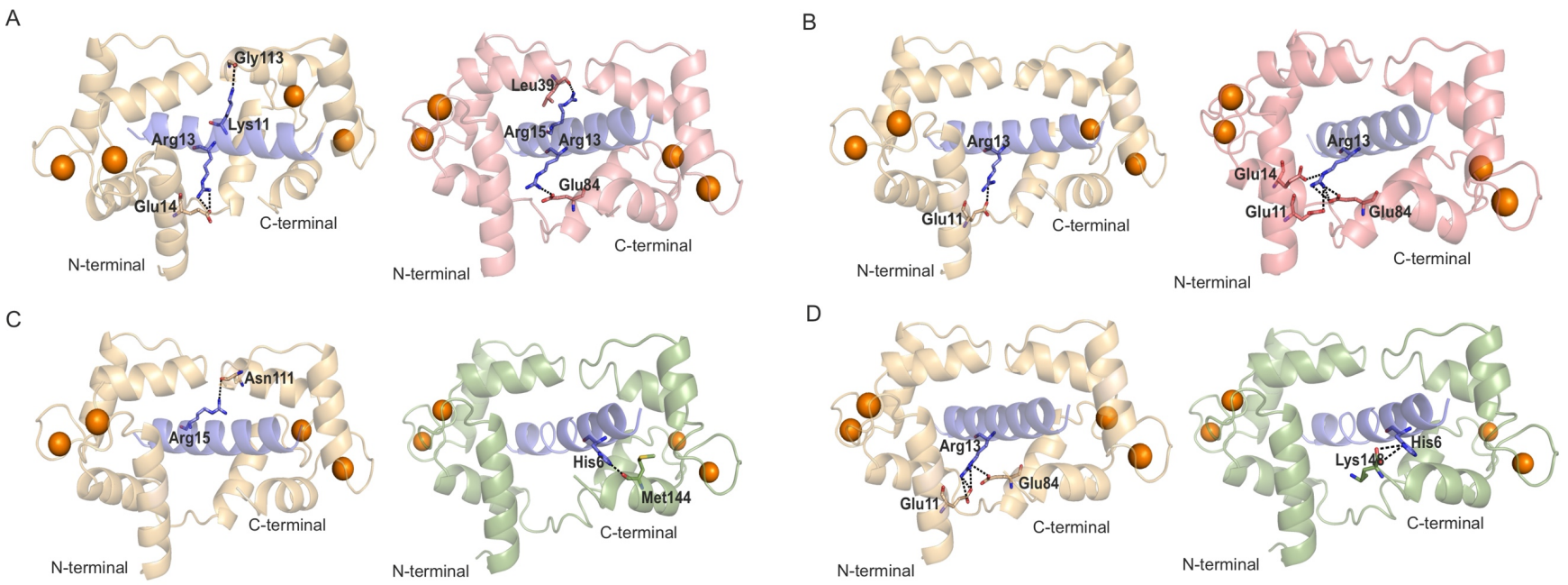

Fig. S3. Comparison of the crystal structures of Ca^{2+}/CaM-WT:$RyR2_{3583-3603}$ (PDB 6XXF), Ca^{2+}/CaM-N53I:RyR2 (PDB 6XY3) and Ca^{2+}/CaM-A102V:$RyR2_{3583-3603}$ (PDB 6XXX). Cartoon representation of (A-B) Ca^{2+}/CaM-WT:$RyR2_{3583-3603}$ (left; CaM in beige and $RyR2_{3583-3603}$ peptide in blue colour) and Ca^{2+}/CaM-N53I: $RyR2_{3583-3603}$ peptide complex (right; CaM-N53I in salmon and RyR2 peptide in blue colour). (C-D) Ca^{2+}/CaM-WT:$RyR2_{3583-3603}$ (left; CaM in beige and $RyR2_{3583-3603}$ peptide in blue colour) and Ca^{2+}/CaM-A102V: $RyR2_{3583-3603}$ peptide complex (right; CaM-A102V in green and RyR2 peptide in blue colour).
Residues from Ca^{2+}/CaM and corresponding peptides involved in (A, C) H-bonds and (B, D) salt bridges unique to each are represented in sticks with interactions marked in black dashed lines. Ca^{2+} ions are represented as orange spheres.
Peptide residues are numbered based on the SI index in Table S4.
$RyR2_{3583-3603}$ (KKAVWHKLLSKQRKRAVVACF) is numbered 1-21. Images were generated using PyMOL software.

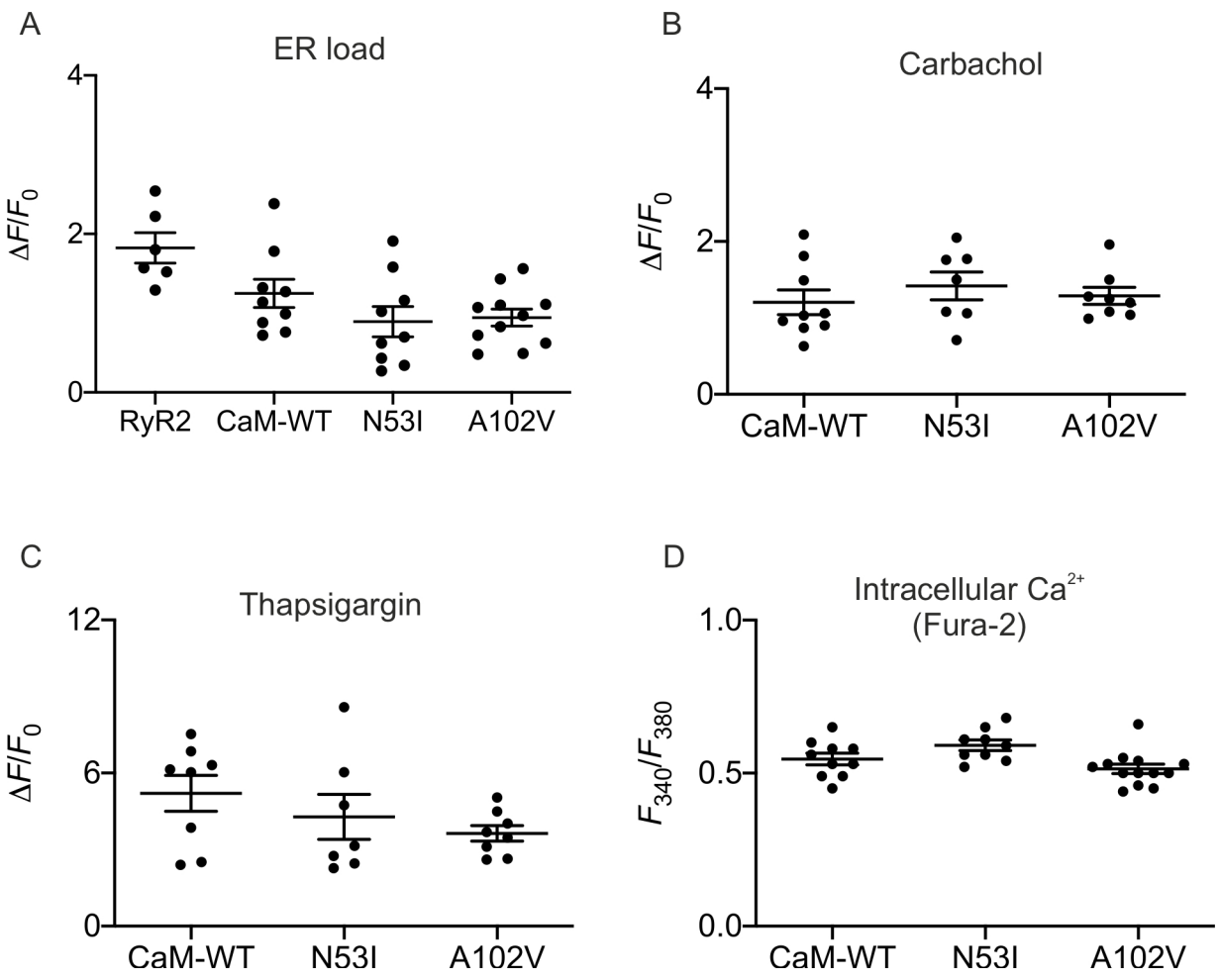

Fig. S4. Over-expression of CaM-WT and CPVT-associated CaM variants did not affect ER-load (caffeine), non-RyR Ca^{2+} response (carbachol, thapsigargin) and intracellular Ca^{2+} concentrations.

(A-C) HEK293T cells transfected with CaM variants ± RyR2 were loaded with Calbryte 520 to monitor intracellular Ca^{2+} concentration changes. Live cells were imaged on a 3i spinning-disk confocal microscope after stimulation with (A) caffeine, (B) carbachol or (C) thapsigargin. (D) HEK293T cells transfected with CaM variants were loaded with Fura-2 to monitor intracellular Ca^{2+} concentration. Live cells were analysed using a Nikon Eclipse epifluorescence microscope and ratiometric imaging.

Data were processed using Fiji and expressed as mean ± SEM. Number of experimental replicates for the ER load experiments (N=dishes) was: N=6 for RyR2, N=9 for RyR2 + CaM-WT, N=9 for RyR2 + CaM-N53I and N=11 for RyR2 + CaM-A102V. Number of experimental replicates for the carbachol experiments (N=dishes) was: N=9 for CaM-WT, N=7 for CaM-N53I and N=8 for CaM-A102V. Number of experimental replicates for the thapsigargin experiments (N=dishes) was: N=8 for CaM-WT, N=7 for CaM-N53I and N=8 for CaM-A102V. Number of experimental replicates for the intracellular Ca^{2+} experiments (N=dishes, n = fields of view) was: N=4, n=10 for CaM-WT; N=3, n=9 for CaM-N53I and N=6, n=13 for CaM-A102V. Differences between groups were determined using one-way ANOVA vs. CaM-WT.

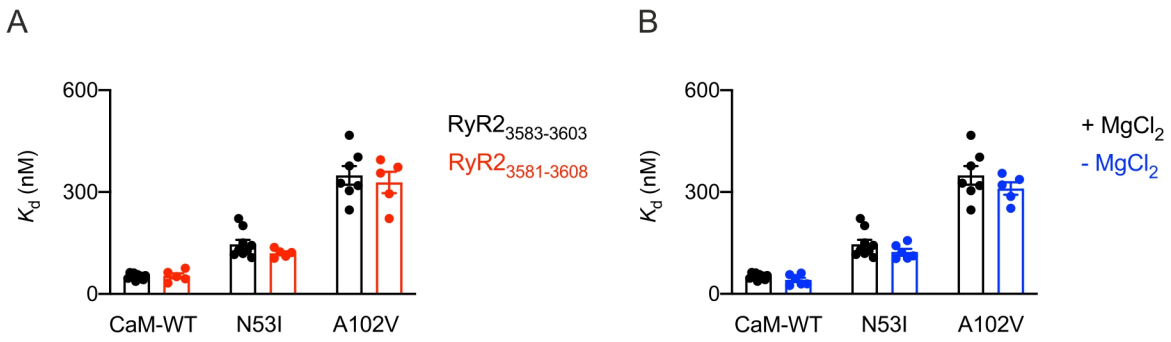

Fig. S5. Effect of peptide length and magnesium concentration on Ca^{2+}/CaM binding to RyR2 using ITC. (A) Affinity of the binding of Ca^{2+}/CaM variants to RyR2$_{3583-3603}$ (short) and RyR2$_{3581-3608}$ (long) obtained by fitting to one-site binding model. (B) Affinity of the binding of Ca^{2+}/CaM variants to RyR2$_{3583-3603}$ in the presence or absence of 2 mM $MgCl_2$ obtained by fitting to one-site binding model Data were processed using the MicroCal PEAQ-ITC software and expressed as mean ± SEM. Experiments were performed at least in 5 replicates, in the presence of 5 mM $CaCl_2$ at 25 °C.

Table S1. The C-lobe of Ca^{2+}/CaM binds first to RyR2. Percentage of residue resonances assigned in the N and C lobes of various ^{15}N-labelled CaM variants from HQSC spectra analysis. Using 0.3 ppm as a threshold, the percentage of assigned resonances which have not significantly shifted in the presence of one molar equivalent $RyR2_{3583-3603}$ peptide are displayed for each CaM lobe (left-hand side). Percentage of assigned resonances which have not significantly shifted upon the addition of $RyR2_{3583-3603}$ peptide from one to two molar equivalents (right-hand side).

CaM-WT	**Unbound – 1.RyR2**		**1.RyR2 – 2.RyR2**	
	% peak assigned	% non-movers	% peak assigned	% non-movers
N-lobe	59.2	57.1	50.7	58.3
C-lobe	36.4	29.2	36.4	91.7

N53I	**Unbound – 1.RyR2**		**1.RyR2 – 2.RyR2**	
	% peak assigned	% non-movers	% peak assigned	% non-movers
N-lobe	45.1	43.8	42.3	56.7
C-lobe	34.9	26.1	33.3	81.8

A102V	**Unbound – 1.RyR2**		**1.RyR2 – 2.RyR2**	
	% peak assigned	% non-movers	% peak assigned	% non-movers
N-lobe	60.6	46.5	49.3	54.3
C-lobe	33.3	18.2	31.8	76.2

Table S2. Data collection and refinement statistics.
Values in brackets are for the last resolution shell.

	Ca^{2+}/CaM-WT:$RyR2_{3583-3603}$	**Ca^{2+}/CaM-N53I:$RyR2_{3583-3603}$**	**Ca^{2+}/CaM-A102V:$RyR2_{3583-3603}$**
Data collection Wavelength (Å)	0.97857	0.97624	0.97624
Beamline	Proxima 1	I03	I03
Detector	Pilatus	Pilatus	Pilatus
Space group	$P2_12_12_1$	$P2_12_12_1$	$P2_12_12_1$
Unit-cell dimensions (*a,b,c*) (Å)	39.92, 41.71, 85.99	39.01, 42.70, 89.36	39.97, 41.67, 85.75
Resolution (Å)	37.56-1.70 (1.70-1.73)	44.72-2.00 (2.00-2.05)	27.34 - 1.23 (1.25 - 1.23)
***Rmerge* %**	9.2 (57.2)	10.0 (36.8)	3.8 (81.6)
***I*/σ (last shell)**	12.5 (6.2)	8.9 (3.8)	18.45 (1.15)
Completeness (%)	100.0 (98.7)	100.0 (100.0)	98.48 (84.19)
Redundancy	5.9 (5.7)	5.3 (5.4)	5.66 (2.65)
Half-set correlation $CC_{1/2}$	0.991 (0.870)	0.994 (0.908)	5.66 (2.65)
No. of reflections	16416	10591	41749
R_{work}/R_{free}	18.0/20.5	20.8/25.9	13.7/19.1
No. of atoms			
Protein	1312	1295	1386
Ca ions	4	4	4
Water	140	50	219
B factor (Å^2)			
Protein	22.63	35.81	24.42
Ca ions	15.87	29.55	19.16
Waters	28.21	32.97	22.45
R.M.S deviations			
Bond length (Å)	0.013	0.008	0.017
Bond angles (°)	1.805	1.457	2.106
PDB code	**6XXF**	**6XY3**	**6XXX**

Table S3. Structural RMSD between various regions of the Ca^{2+}/CaM-WT:$RyR2_{3583-3603}$ peptide complex and the Ca^{2+}/CaM-N53I:$RyR2_{3583-3603}$, Ca^{2+}/CaM-A102V:$RyR2_{3583-3603}$ peptide complex crystal structures.
RMSD values were obtained using PyMOL "super" command.

Ca^{2+}/CaM-WT:$RyR2_{3583-3603}$	**Ca^{2+}/CaM-N53I:$RyR2_{3583-3603}$ RMSD (Å)**	**Ca^{2+}/CaM-A102V:$RyR2_{3583-3603}$ RMSD (Å)**
Full complex	1.31	0.63
N-terminal region (residue 6 - 65)	0.90	0.72
Flexible helix (residue 66 - 93)	1.43	0.77
C-terminal region (residue 94 - 149)	0.77	0.52
$RyR2_{3583-3603}$ peptide	1.13	0.21

Table S4. Residues involved in H-bond and salt bridge interactions between $RyR2_{3583-3603}$ peptide and Ca^{2+}/CaM-WT, Ca^{2+}/CaM-N53I and Ca^{2+}/CaM-A102V. Data were obtained using PDBePISA server.

		H-bond interactions			Salt bridge interactions		
SI.	$RyR2_{3583-3603}$	Ca^{2+}/CaM-WT	Ca^{2+}/CaM-N53I	Ca^{2+}/CaM-A102V	Ca^{2+}/CaM-WT	Ca^{2+}/CaM-N53I	Ca^{2+}/CaM-A102V
1	Lys3583	Glu123; Glu127	Glu127[1]	Glu123; Glu127	Glu123; Glu127	Glu127[1]	Glu123; Glu127
2	Lys3584	Glu127	Glu127	Glu127	-	-	-
3	Ala3585	-	-	-	-	-	-
4	Val3586	-	-	-	-	-	-
5	Trp3587	Met124	Met124	Met124	-	-	-
6	His3588	-	-	Met144	-	-	Lys148
7	Lys3589	Glu114	Glu114	Glu114	Glu114	Glu114	Glu114
8	Leu3590	-	-	-	-	-	-
9	Leu3591	-	-	-	-	-	-
10	Ser3592	-	-	-	-	-	-
11	Lys3593	Leu112; Gly113; Glu114	Leu112; Glu114	Leu112; Gly113; Glu114	Glu114	Glu114	Glu114
12	Gln3594	-	-	-	-	-	-
13	Arg3595	Glu11; Glu14	Glu11; Glu84	Glu11; Glu14	Glu11; Glu14; Glu84	Glu11; Glu14; Glu84	Glu14; Glu84
14	Lys3596	-	-	-	-	-	-
15	Arg3597	Asn111	Leu39; Asn111	-	-	-	-
16	Ala3598	-	-	-	-	-	-
17	Val3699	-	-	-	-	-	-
18	Val3600	-	-	-	-	-	-
19	Ala3601	-	-	-	-	-	-
20	Cys3602	Lys75	-[2]	Lys75	-	-	-
21	Phe3603	-	-	-	-	-	-

[1] Glu123 side-chain atoms are not resolved in the structure

[2] Lys75 side-chain atoms are not resolved in the structur